Draft version July 9, 2025
Typeset using LaTeX **manuscript** style in AASTeX631

Helicity Fluxes and Hemispheric Helicity Rule of Active Regions Emerging from the Convection Zone Dynamo

Valery V. Pipin [1,2] Shangbin Yang [1] and Alexander G. Kosovichev [3]

[1] *National Astronomical Observatories, Chinese Academy of Sciences, 20A Datun Road, Chaoyang District, Beijing, China*

[2] *Institute of Solar-Terrestrial Physics, Russian Academy of Sciences, Irkutsk, 664033, Russia*

[3] *New Jersey Institute of Technology, Newark, NJ 07102, USA*

Submitted to ApJ

ABSTRACT

Using a 3D non-linear mean-field solar dynamo model, we investigate the magnetic helicity flux and magnetic twist and tilt parameters of bipolar magnetic regions (BMRs) emerging from the solar convection zone due to the magnetic buoyancy instability. The twist and tilt of the BMR magnetic field are modeled as a result of an effective electromotive force along the rising part of the toroidal magnetic field. This force generates the poloidal field that tilts the whole magnetic configuration. We find that variations of BMR's twist and tilt determine the magnitude and sign of the magnetic helicity flux on the solar surface. The model shows that the helicity flux associated with the BMR's tilt/twist is the dominant contribution to the BMR helicity at the beginning of the BMR's evolution, while the effect of differential rotation is the main source of the helicity flux at the final stage of the BMR's evolution. We discuss the implications of these effects on the basic properties and variations of the hemispheric helicity rule of active regions on the solar surface.

Keywords: Sun: dynamo –Sun: magnetic topology

1. INTRODUCTION

Magnetic helicity balance plays an important role in the dynamo processes in the solar and stellar convection zones. In particular, the nonlinear saturation of the turbulent dynamo significantly depends on the evolution of the magnetic helicity and its expulsion from the dynamo domain (Kleeorin & Ruzmaikin 1982; Brandenburg et al. 2023). Moreover, the magnetic helicity flux from the depth of the convection zone can affect the activity phenomena in the chromosphere and corona. For example, the amount of helicity stored in solar active regions affects their flare and coronal mass ejection (CME) productivity (e.g., Berger & Ruzmaikin 2000; Pariat et al. 2009; Georgoulis et al. 2009; Toriumi & Wang 2019).

It was found that the solar differential rotation provides a major effect on the rate of helicity production, both in the flaring and CME activity of individual active regions and in the progression of solar activity cycles (Berger & Ruzmaikin 2000; Hawkes & Yeates 2019). This supports the basic dynamo scenario of Parker (1955), suggesting that the differential rotation and turbulent generation of large-scale magnetic fields are the main sources of the magnetic energy generated in the solar dynamo. This model predicted that the dynamo-generated magnetic field migrates in radius and latitude in the form of dynamo waves. It showed that magnetic stresses and modulation of the turbulent heat flux, associated with these waves, **result in 11-year variations of the differential rotation ("torsional oscillations") which are featured by an extended 22-year mode propagating during two solar cycles from the polar regions to the equator (Kosovichev & Pipin 2019; Pipin & Kosovichev 2019; Mandal et al. 2024). Similarly, the model reproduces variations of the meridional circulation, also in agreement with helioseismology results (e.g., Komm et al. 2018; Pipin & Kosovichev 2020; Getling et al. 2021; Getling & Kosovichev 2025).**

The emergence of the tilted bipolar magnetic regions (BMR), together with the effects of the cyclonic convection motions (associated with the so-called α-effect), represents the turbulent dynamo generation of the large-scale magnetic field observed on the surface of the Sun. **Both effects are related to the production of the helical magnetic field and therefore affect the magnetic helicity fluxes from the solar convection zone.** Previous studies (e.g., Kleeorin et al. 2000; Blackman & Brandenburg 2003; Brandenburg & Subramanian 2005) suggested an important role for turbulent magnetic helicity fluxes for the large-scale dynamo.

Another important aspect of the problem is the hemispheric helicity rule (hereafter HHR). It states that the electric current helicity, which is a proxy of magnetic helicity, is predominantly negative in the Northern hemisphere and positive in the Southern hemisphere. In other words, the magnetic field of bipolar magnetic regions (BMRs) is twisted counter-clockwise in the Northern hemisphere and clockwise in the Southern hemisphere. Starting from the results of Seehafer (1990), Pevtsov et al. (1994) and Bao & Zhang (1998), the hemispheric helicity rule is a well-established statistical pattern of the solar active regions. However, there are significant fluctuations (Zhang et al. 2024). In particular, observations show that solar active regions can violate the hemispheric helicity rule mostly during the initial phase of active region emergence (Kutsenko et al. 2019). The mean-field dynamo models attempt to relate the HHR with the sign of the α-effect and magnetic helicity conservation (Sokoloff et al. 2006; Pipin et al. 2013). The surface flux-transport models interpret observations of the HHR in a different way. For example, Prior & Yeates (2014) modeled HHR as an effect of the differential rotation acting on the initial random distribution of the helical BMRs. The reader can find more information on solar magnetic helicity and beyond in reviews published in Kuzanyan et al. (2024). Using a surface flux-transport model, Hawkes & Yeates (2019) found that the magnitude of the helicity flux due to the decay of active regions is about two orders of magnitude lower than that of the helicity flux produced by the differential rotation. However, the flux-transport models do not take into account the radial dependence of the magnetic field distributions and the BMR emergence in the convection zone (Yeates et al. 2023; Pipin 2024). This can lead to an underestimation of the BMR role in the magnetic helicity budget and consequently the helicity flux from the photosphere to the solar corona. Nevertheless, it is important that the magnetic helicity flux, initiated by the BMR's emergence and evolution, and the HHR can be closely related.

Our general goal is to evaluate the contribution of BMRs to the total magnetic helicity balance. For this purpose, we use the non-linear 3D MHD dynamo model of Pipin et al. (2023), which addresses the emergence and evolution of BMR simultaneously with the global dynamo in the solar convection zone. We calculate the helicity flux initiated by BMRs and also the latitudinal distribution of the magnetic twist parameters of BMRs. The dynamo model allows us to estimate directly the contributions of the helicity production rate on the solar surface caused by the large-scale flows and the evolution of the bipolar active regions. Our plan is as follows. Section 2 discusses some aspects of the dynamo model and the evolution equation for the helicity rate. In Section 3, we calculate the surface helicity flux using typical configurations for emerging BMRs. Then, we calculate the HHR for the BMR's twist parameters and helicity flux. The paper ends with a discussion and conclusions.

2. MAGNETIC HELICITY BALANCE

The total magnetic helicity inside the convection zone can be defined via the volume integral,

$$\mathcal{H}_V = \int \boldsymbol{A} \cdot \boldsymbol{B} \mathrm{dV}, \tag{1}$$

where $\boldsymbol{A}$ is the magnetic vector potential, $\boldsymbol{B} = \nabla \times \boldsymbol{A}$. **Hereafter, we assume the volume integral is calculated over the bulk of the convection zone.** Generally, the vector-potential is defined only up to a gauge transformation, $\boldsymbol{A} \rightarrow \boldsymbol{A} + \boldsymbol{\nabla} g$, where g is an arbitrary scalar. For the large-scale dynamo models, the uncertainty is cured by the decomposition of the magnetic field into a sum of the toroidal, $\boldsymbol{B}_T$, and poloidal components, $\boldsymbol{B}_P$, (Krause & Rädler 1980), which are decomposed further following Chandrasekhar & Kendall (1957):

$$\boldsymbol{B} = \boldsymbol{B}_T + \boldsymbol{B}_P = \boldsymbol{\nabla} \times \boldsymbol{r} T(\boldsymbol{r}, t) + \boldsymbol{\nabla} \times \boldsymbol{\nabla} \times \boldsymbol{r} S(\boldsymbol{r}, t) \tag{2}$$

where the first term in the RHS corresponds to $\boldsymbol{B}_T$, and T and S are scalars, which are called superpotentials. The superpotentials also have gauge uncertainty. However, in this case, the arbitrary scalars, which take part in the gauge transformation, depend on the radial coordinate only. This uncertainty can be removed if we consider the appropriate integral averaging of T and S. The procedure is particularly simple in the

case of the spherical dynamo models, see more details in Appendix A and the book by Krause & Rädler (1980). The helicity integral, $\mathcal{H}_V$, measures the linkage of, $\boldsymbol{B}_T$ and $\boldsymbol{B}_P$ in the volume (Berger & Hornig 2018).

We employ the Electromagnetic units system throughout the paper, and following the Faraday law,

$$\frac{\partial \boldsymbol{B}}{\partial t} = -\nabla \times \boldsymbol{E}, \tag{3}$$

where $\boldsymbol{E}$ is the electric field, determine the helicity rate in the bulk of the convection zone:

$$\frac{\mathrm{d}\mathcal{H}_V}{\mathrm{d}t} = \int \left(\frac{\partial \boldsymbol{A}}{\partial t} \cdot \boldsymbol{B} + \boldsymbol{A} \cdot \frac{\partial \boldsymbol{B}}{\partial t}\right) \mathrm{dV} = \int \left(2\boldsymbol{A} \cdot \frac{\partial \boldsymbol{B}}{\partial t} + \nabla \cdot \left(\boldsymbol{A} \times \frac{\partial \boldsymbol{A}}{\partial t}\right)\right) \mathrm{dV} \tag{4}$$

$$= -2 \int \boldsymbol{E} \cdot \boldsymbol{B} dV + 2 \oint d\boldsymbol{S} \cdot (\boldsymbol{A} \times \boldsymbol{E}) + \oint d\boldsymbol{S} \cdot \left(\boldsymbol{A} \times \frac{\partial \boldsymbol{A}}{\partial t}\right). \tag{5}$$

It is noteworthy that the last integral in this formula is identically zero (Berger & Hornig 2018). We keep it because in the dynamo equations, $\left(\boldsymbol{A} \times \frac{\partial \boldsymbol{A}}{\partial t}\right)$ has a counterpart in $(\boldsymbol{A} \times \boldsymbol{E})$. Taking into account Ohm's law,

$$\boldsymbol{E} = -\boldsymbol{v} \times \boldsymbol{B} + \eta \boldsymbol{J}, \tag{6}$$

where $\boldsymbol{v}$ is the plasma velocity, $\boldsymbol{J}$ is the electric current density, and η is the microscopic diffusivity, we get the helicity rate in the volume of the convection zone:

$$\frac{\mathrm{d}\mathcal{H}_V}{\mathrm{d}t} = -2\eta \int \boldsymbol{B} \cdot \boldsymbol{J} dV + 2 \oint d\boldsymbol{S} \cdot \boldsymbol{B} \left(\boldsymbol{A} \cdot \boldsymbol{v}\right) - 2 \oint d\boldsymbol{S} \cdot \boldsymbol{v} \left(\boldsymbol{A} \cdot \boldsymbol{B}\right) \tag{7}$$

$$+ 2\eta \oint d\boldsymbol{S} \cdot (\boldsymbol{A} \times \boldsymbol{J}) + \oint d\boldsymbol{S} \cdot \left(\boldsymbol{A} \times \frac{\partial \boldsymbol{A}}{\partial t}\right). \tag{8}$$

Next, following the standard approach of the mean-field magnetohydrodynamics, we decompose the induction vector of the magnetic field, $\boldsymbol{B}$, and its vector-potential $\boldsymbol{A}$, into the mean and fluctuating parts,

$$\boldsymbol{B} = \langle \boldsymbol{B} \rangle + \boldsymbol{b}, \tag{9}$$

$$\boldsymbol{A} = \langle \boldsymbol{A} \rangle + \boldsymbol{a},$$

$$\boldsymbol{v} = \langle \boldsymbol{U} \rangle + \boldsymbol{u},$$

$$\boldsymbol{J} = \langle \boldsymbol{J} \rangle + \boldsymbol{j}$$

where the small letters denote the turbulent fluctuations and the angular brackets denote the averaging over the ensemble of fluctuations. Substituting these decompositions into Eq.(5) and averaging over the ensemble of fluctuations, we get,

$$\frac{\mathrm{d}\mathcal{H}_V}{\mathrm{d}t} = \frac{\mathrm{d}}{\mathrm{d}t}\int \left(\langle \boldsymbol{a}\cdot\boldsymbol{b}\rangle + \langle \boldsymbol{A}\rangle \cdot \langle \boldsymbol{B}\rangle\right)\mathrm{d}V = -2\eta \int \left(\langle \boldsymbol{b}\cdot\boldsymbol{j}\rangle + \left(\langle \boldsymbol{B}\rangle \cdot \langle \boldsymbol{J}\rangle\right)\right)\mathrm{d}V \tag{10}$$
$$- \oint d\boldsymbol{S}\cdot \boldsymbol{F}^{\langle ab\rangle} + 2\eta \oint d\boldsymbol{S}\cdot \left(\langle \boldsymbol{a}\times\boldsymbol{j}\rangle + \langle \boldsymbol{A}\rangle \times \langle \boldsymbol{J}\rangle\right) + \oint d\boldsymbol{S}\cdot\left(\langle \boldsymbol{A}\rangle \times \frac{\partial \langle \boldsymbol{A}\rangle}{\partial t}\right),$$

where $\boldsymbol{F}^{\langle ab\rangle}$ is the flux of the turbulent magnetic helicity density, $\langle \boldsymbol{a}\cdot\boldsymbol{b}\rangle$. **This equation shows that the total helicity rate in the volume is only due to the Ohmic dissipation of the current helicity, and the turbulent helicity flux $\boldsymbol{F}^{\langle ab\rangle}$ through the dynamo domain boundaries.** In the mean-field theory, the general expression of $\boldsymbol{F}^{\langle ab\rangle}$ is complicated (see, Kleeorin & Rogachevskii 2022; Gopalakrishnan & Subramanian 2023). It includes the products of the large-scale flow, $\langle \boldsymbol{U}\rangle$, magnetic field, $\langle \boldsymbol{B}\rangle$ and its vector potential $\langle \boldsymbol{A}\rangle$ with the second moments of the turbulent fields, and the triple-order moments of the turbulent fields. In our study, we approximate it by the effect of turbulent diffusion,

$$\boldsymbol{F}^{\langle ab\rangle} = -\eta_{\chi}\boldsymbol{\nabla}\left\langle \boldsymbol{a}\cdot\boldsymbol{b}\right\rangle. \tag{11}$$

Following the results of Mitra et al. (2010); Kleeorin & Rogachevskii (2022), we set $\eta_{\chi} = \frac{1}{10}\eta_T$, where η_T is the amplitude of the magnetic eddy diffusivity. The latter is determined with the help of the analytical results of the mean-field theory and the standard mixing-length approximation for the convective zone turbulent flows. **Except for $\boldsymbol{F}^{\langle ab\rangle}$, the second line of Eq.(10) contains the Fickian-type fluxes of the small-scale and large-scale helicity due to the Ohmic diffusion, i.e., the contributions like, $\eta\boldsymbol{\nabla}\left\langle \boldsymbol{a}\cdot\boldsymbol{b}\right\rangle$ and $\eta\boldsymbol{\nabla}\left\langle \boldsymbol{A}\right\rangle\cdot\left\langle \boldsymbol{B}\right\rangle$ (cf., Eq.(23) and Sec. 3). However, these contributions are much smaller in comparison to the turbulent diffusion, and, therefore, we neglect them in our analysis.**

The evolution equation for the small-scale helicity can be obtained from Eq(10) using the mean-field induction equation,

$$\frac{\partial \langle \boldsymbol{B}\rangle}{\partial t} = \nabla \times \left(\boldsymbol{\mathcal{E}} + \langle \boldsymbol{U}\rangle \times \langle \boldsymbol{B}\rangle\right), \tag{12}$$

where $\boldsymbol{\mathcal{E}} = \langle \boldsymbol{u} \times \boldsymbol{b} \rangle$ is the mean electromotive force of the turbulent flows. We describe the mathematical details in Appendix A. The final result is as follows,

$$\begin{aligned}\frac{\mathrm{d}}{\mathrm{d}t}\int \langle \boldsymbol{a}\cdot\boldsymbol{b}\rangle\, dV = & -2\int \left(\boldsymbol{\mathcal{E}}\cdot\langle\boldsymbol{B}\rangle\right) dV - \int \frac{\langle \boldsymbol{a}\cdot\boldsymbol{b}\rangle}{R_m\tau_c} dV + 2\eta\oint d\boldsymbol{S}\cdot\langle\boldsymbol{a}\times\boldsymbol{j}\rangle \\ & -\oint d\boldsymbol{S}\cdot\boldsymbol{F}^{\langle ab\rangle} + \oint d\boldsymbol{S}\cdot\langle\boldsymbol{U}\rangle\left(\langle\boldsymbol{A}\rangle\cdot\langle\boldsymbol{B}\rangle\right) \\ & -2\oint d\boldsymbol{S}\cdot\left(\boldsymbol{\mathcal{E}}\times\langle\boldsymbol{A}\rangle\right) - 2\oint d\boldsymbol{S}\cdot\langle\boldsymbol{B}\rangle\left(\langle\boldsymbol{A}\rangle\cdot\langle\boldsymbol{U}\rangle\right),\end{aligned} \tag{13}$$

where, R_m is the turbulent magnetic Reynolds number, τ_c is the typical convective turnover time of the turbulent flows. Here, we employ the result of Kleeorin & Rogachevskii (1999) for isotropic turbulence, $2\eta\langle\boldsymbol{b}\cdot\boldsymbol{j}\rangle = \frac{\langle \boldsymbol{a}\cdot\boldsymbol{b}\rangle}{R_m\tau_c}$. In this study, we assume that the normal to the surface component of the large-scale flow, $\langle\boldsymbol{U}\rangle$, is zero at the top boundary. The term -2$\oint d\boldsymbol{S}\cdot(\boldsymbol{\mathcal{E}}\times\langle\boldsymbol{A}\rangle)$ represents the helicity flux initiated by the turbulent processes in the large-scale dynamo. Pipin et al. (2013) found that this helicity flux results in the small-scale magnetic helicity density evolution following the large-scale dynamo wave. This alleviates the non-linear saturation (catastrophic quenching) of the α-effect. Del Sordo et al. (2013) and Brandenburg (2018) investigated this flux using direct numerical simulations and found that it was difficult to confirm this effect due to the limited numerical resolution. The term $-2\oint d\boldsymbol{S}\cdot\langle\boldsymbol{B}\rangle\left(\langle\boldsymbol{A}\rangle\cdot\langle\boldsymbol{U}\rangle\right)$ stands for effects of the large-scale flow, i.e., the differential rotation and meridional circulation (Berger & Ruzmaikin 2000; Hawkes & Yeates 2019). Our goal is to study the contribution of the bipolar active regions to these helicity fluxes.

To achieve this goal, we consider the dynamo model with emerging active regions proposed by Pipin et al. (2023). In this model, the evolution equation for the mean magnetic induction vector, $\langle\boldsymbol{B}\rangle$, describes both the dynamo-generated large-scale magnetic field and the magnetic field of active regions that are formed from the large-scale toroidal magnetic field due to the magnetic buoyancy instability. Such formulation of the mean-field dynamo model is possible by considering mean nonaxisymmetric magnetic fields. In the model, we approximate the magnetic configurations of active regions in the form of bipolar magnetic structures. Observations show that the contribution of bipolar-like active regions to the total unsigned flux of the photospheric radial magnetic fields is less than 10 percent (Nagovitsyn et al. 2016; Pevtsov et al. 2021). Moreover, the flux distribution in the solar active regions shows a rich diversity of the magnetic patterns (Abramenko et al. 2023). The above arguments show the limitations and the main source of uncertainty in the comparison of the model with observations.

We consider the mean magnetic field induction equation (Eq. 12) for the highly conductive media with the addition of the effects of the bipolar magnetic regions. In this equation, the electromotive force $\mathcal{E}$ contains both the mean-field turbulent effects and the generation terms for BMRs, defined in Appendix A and the next section. The mean large-scale flow velocity, $\langle \boldsymbol{U} \rangle$, represents the differential rotation and the meridional circulation. It is calculated consistently by solving Eq. (12) together with the equations that describe the angular momentum balance, the meridional circulation, the mean-field heat transport, and the integral balance of the magnetic helicity in the bulk of the solar convection zone (Pipin & Kosovichev 2024). We use the harmonic field approximation (Bonanno 2016) outside the dynamo domain, which is more suitable for modeling the magnetic helicity because, unlike the usual potential field approximation, it does not suppress the contributions from the tilt and twist of BMRs on the surface. In this case, we employ the standard boundary conditions: continuity of the normal component of the magnetic field and the tangential component of the mean electromotive force (see Appendix B).

3. MODEL OF TILTED/TWISTED BIPOLAR MAGNETIC REGIONS

The mean electromotive force, $\boldsymbol{\mathcal{E}} = \langle \boldsymbol{u} \times \boldsymbol{b} \rangle$, represents the effects of turbulent flows and magnetic fields on the large-scale magnetic field induction. We formulate it as follows,

$$\mathcal{E}_i = (\alpha_{ij} + \gamma_{ij}) \langle B \rangle_j - \eta_{ijk} \nabla_j \langle B \rangle_k + \mathcal{E}_i^{(\mathrm{BMR})}, \tag{14}$$

where α_{ij} describes the turbulent generation by the hydrodynamic magnetic helicity (the global dynamo α-effect), γ_{ij} is the turbulent pumping, η_{ijk} is the eddy magnetic diffusivity tensor, and $\boldsymbol{\mathcal{E}}^{(\mathrm{BMR})}$ models the emergence of the tilted/twisted bipolar active regions, see details in Appendix A. The additional term of the mean electromotive force, $\boldsymbol{\mathcal{E}}^{(\mathrm{BMR})}$, is formulated as follows (Pipin et al.

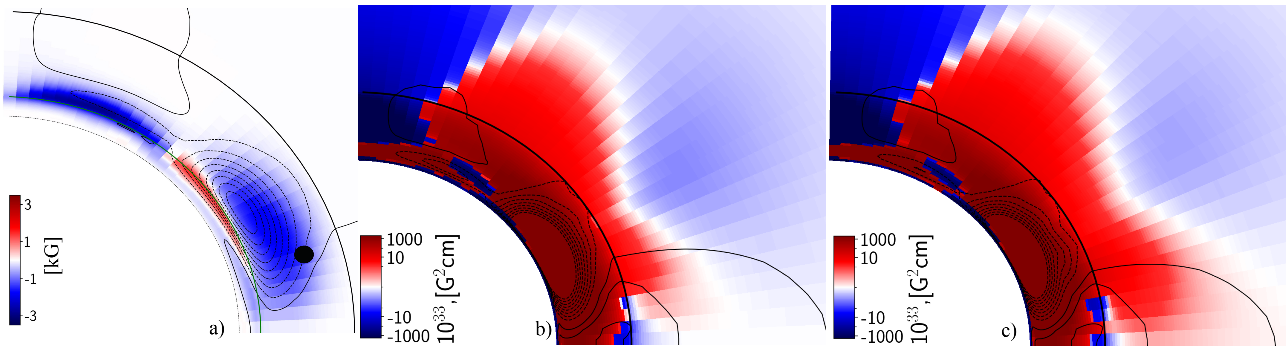

Figure 1. A snapshot of the large-scale axisymmetric magnetic field and magnetic helicity density in the northern hemisphere of the Sun: a) the color image shows the toroidal magnetic field, and the contour lines of the axisymmetric vector potential show the poloidal magnetic field lines; the black circle shows the position of the BMR initiation; b) the color image show the magnetic helicity density of axisymmetric magnetic field at the same time as in panel (a), and the contour lines are the same as in panel (a)); c) the same as b) at the end of the run E6, which included the initial axisymmetric poloidal magnetic field, see Table 1.

2023):

$$\boldsymbol{\mathcal{E}}^{(\mathrm{BMR})}=\alpha_{\beta}^{\mathrm{BMR}}\left\langle \boldsymbol{B}\right\rangle +V_{\beta}\left(\hat{\boldsymbol{r}}\times\left\langle \mathbf{B}\right\rangle \right), \tag{15}$$

where the first term takes into account the BMR's tilt/twist and the second term models the rise of the magnetic region to the surface in the bipolar form with velocity V_{β}. In our basic scenario, the term $\alpha_{\beta}^{\mathrm{BMR}}\left\langle B_{\phi}\right\rangle$ induces an effective electromotive force along the rising part of the toroidal magnetic field. This electromotive force generates the poloidal magnetic field, which tilts the whole magnetic configuration of BMR. If we leave the toroidal magnetic field at rest (no rise), then this additional small-scale poloidal magnetic field results in the twisted magnetic field configuration. Therefore, it makes sense to divide the BMR formation process, described by Eq. (15), into the two corresponding parts:

$$\boldsymbol{\mathcal{E}}^{(\mathrm{BMR})}=\boldsymbol{\mathcal{E}}_{1}+\boldsymbol{\mathcal{E}}_{2}, \tag{16}$$

$$\boldsymbol{\mathcal{E}}_{1}=\alpha_{\beta}^{\mathrm{BMR}}\left\langle \boldsymbol{B}\right\rangle \xi_{1}(t,\boldsymbol{r})$$

$$\boldsymbol{\mathcal{E}}_{2}=V_{\beta}\left(\hat{\boldsymbol{r}}\times\left\langle \mathbf{B}\right\rangle \right)\xi_{2}(t,\boldsymbol{r})$$

where functions ξ_1 and ξ_2 describe the spatio-temporal parameters of the initial perturbations of the magnetic buoyancy instability. The magnetic buoyancy velocity, V_β, includes the turbulent and mean-field buoyancy effects (Kitchatinov & Pipin 1993):

$$V_\beta = \frac{\alpha_{\rm MLT} u_c}{\gamma} \beta^2 \mathcal{H}(\beta) \tag{17}$$

where function $\mathcal{H}(\beta)$ describes the quenching effect of the magnetic tension (see the above-cited paper). Also, $\alpha_{\rm MLT} = 1.9$ is the mixing length theory parameter, u_c is the RMS convective velocity, and γ is the adiabatic constant. All these parameters are taken from the results of the standard MESA model for the Sun (Paxton et al. 2011). Following Pipin (2022), we define

$$\alpha_\beta^{\rm BMR} = C_{\alpha\beta} \cos\theta V_\beta \psi_\alpha(\beta). \tag{18}$$

Here, the parameter $C_{\alpha\beta}$ determines the magnitude of tilt/twist of the BMR for a given latitude. The function, $\psi_\alpha(\beta)$, where $\beta = \left|\langle\mathbf{B}\rangle\right| / \sqrt{4\pi\overline{\rho}\mathrm{u_c^2}}$, describes the algebraic quenching of the α effect. We define the functions $\xi_{1,2}(t, \mathbf{r})$ in the same way as Pipin et al. (2023). Their description is given in Appendix C. **A similar form of the α-effect was suggested earlier by Ferriz-Mas et al. (1994). In our model, the typical amplitude of $\alpha_\beta^{\rm BMR}$ is about 5-10 m/s. This is of the same order of magnitude as the global dynamo α-affect in the upper part of the convection zone (see Figure 3 in Pipin 2022). According to Choudhuri (1992) and Hoyng (1993), such strong fluctuations can be possible if we take into account the local character of the BMR's formation.**

We did not investigate whether this effect could generate a large-scale dynamo on its own. Clearly, a solar-like BMR can be produced when a sufficiently strong seed toroidal magnetic field is present. Its action on a weak poloidal field is consistent with the standard mean-field α effect. Pipin (2022) found that for a given parameter $C_{\alpha\beta}$, the amplitudes of the poloidal and toroidal magnetic fields produced by the BMRs are larger by about ten percent of their values in the mean-field global axisymmetric dynamo model without BMRs for the same α-effect parameter $C_{\alpha\beta}$.

Depending on the mutual phase of $\boldsymbol{\mathcal{E}}_1$ and $\boldsymbol{\mathcal{E}}_2$, the sign of $C_{\alpha\beta}$ and the employed boundary conditions, we can distinguish several interesting cases for the study. We assume that the emergence phase, which is associated with magnetic buoyancy, $\boldsymbol{\mathcal{E}}_2$, can start either after the action of $\boldsymbol{\mathcal{E}}_1$ or simultaneously with it. When $\boldsymbol{\mathcal{E}}_1$ precedes $\boldsymbol{\mathcal{E}}_2$, it results in the rise of a twisted bipolar magnetic field structure. The simultaneous action of $\boldsymbol{\mathcal{E}}_1$ and $\boldsymbol{\mathcal{E}}_2$ produces a tilted and twisted BMR. We can vary the sign and phase of $\boldsymbol{\mathcal{E}}_1$ to generate the different signs of twist and tilt. We list the cases in Table 1.

For the source of the BMR initiation, we considered the toroidal magnetic field in the upper part of the convection zone at the growing stage of the dynamo cycle, where the condition for the magnetic buoyancy instability is satisfied (Pipin et al. 2023). Snapshots of the large-scale magnetic field and its helicity density distributions before and after the BMR's emergence are shown in Figure 1, as an example. **In the model, the large-scale magnetic field is almost antisymmetric about the equator. This is because the dynamo model employs the mean-field alpha effect, which is slightly above the dynamo instability threshold when the quadrupolar modes are still subcritical. The nonlinear dynamo processes, as well as spontaneous BMR formation can break the parity of the magnetic field during the solar cycle. This can also affect the helicity fluxes. Here, we ignore these effects and consider the magnetic helicity parameters for a particular stage of the solar cycle with an almost antisymmetric configuration of the large-scale magnetic field. The latitude of the initial perturbation shown by the black circle is fixed at 20°. Inside the convection zone, the helicity density shows opposite signs at low and high latitudes. These signs propagate out of the dynamo region. We made one of the runs using setup E6 (Table 1) and taking into account the full axisymmetric magnetic field. Figures 1(b and c) show snapshots of the axisymmetric magnetic field helicity density at the beginning and at the end of the run. This run (E6) employs the harmonic boundary conditions. In the northern hemisphere we see the injection of the positive helicity that at the end of the run. Also, the helicity density in the low corona changes in the near-equatorial regions. Similarly to the results of Warnecke et al. (2011); Bonanno (2016); Bourdin et al. (2018), the magnetic helicity density**

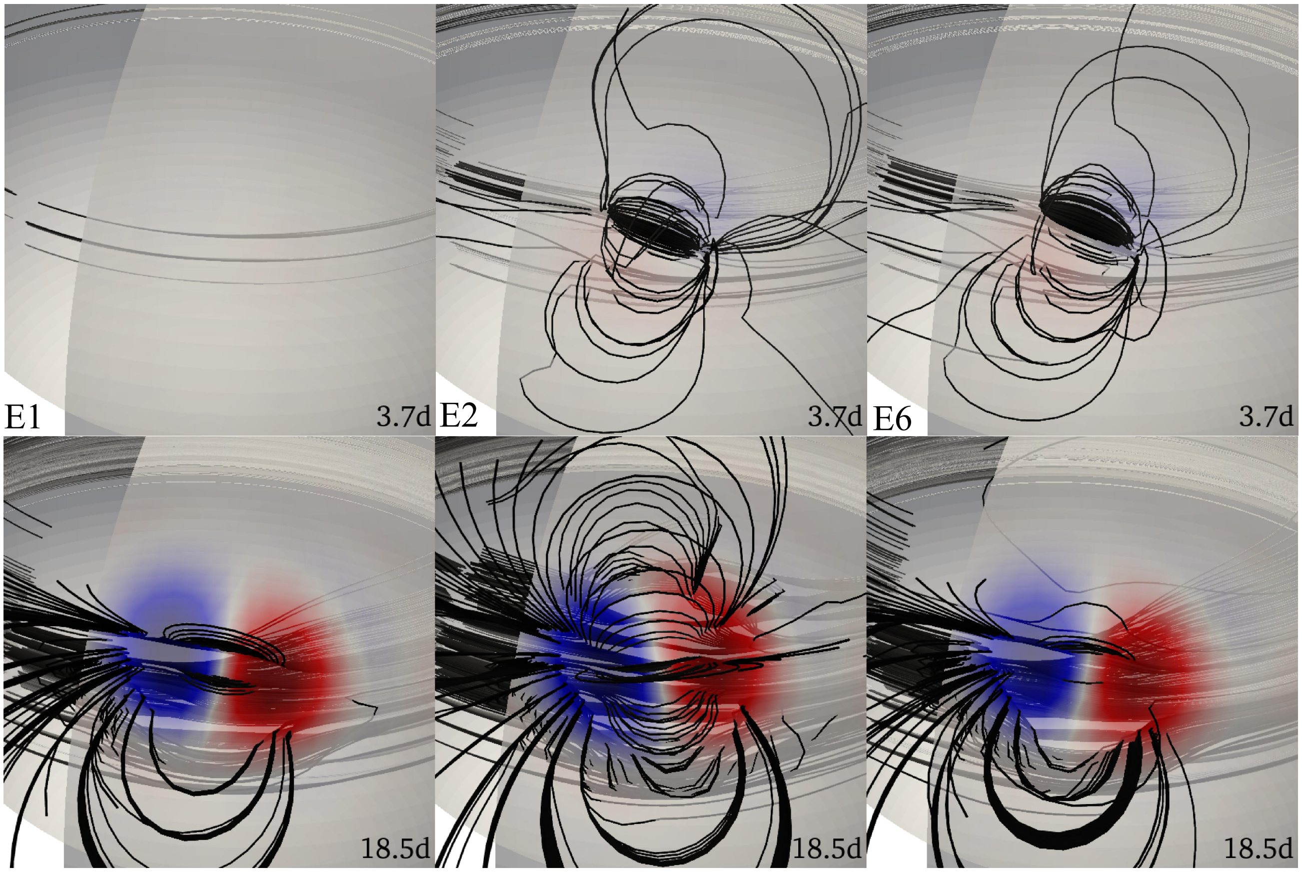

Figure 2. The top row shows the snapshots of the magnetic field distribution in a bipolar magnetic region (BMR) at the beginning of its emergence at the surface. The bottom row shows the same for the final stage of the simulation. The columns marked E1, E2, and E6 correspond to the cases listed in Table 1. The color image shows the radial magnetic field. **The online version contains an animation of this Figure. The animation illustrates the magnetic field evolution of BMRs, spanning 2 to 19 days, during the evolution of the active regions.**

of the axisymmetric magnetic field shows an inversion of sign at radius $r \approx 1.7R_{\odot}$. This effect was found in the analysis of solar wind observations by Brandenburg et al. (2011). We leave a detailed study of this problem for another paper. To exclude the effects of interaction of the magnetic field of BMR with the axisymmetric poloidal magnetic field that may exist before the BMR's emergence, we set the initial axisymmetric poloidal magnetic field strength. For models E5 and E6, we make additional runs varying the initiation latitude of the BMR initiation in the range $\pm 40^{\circ}$.

Table 1. Parameters of the runs.

Case	Type BMR	BC	$\mathcal{E}_1$ (α-effect)	$\mathcal{E}_2$ (buoyancy)	$C_{\alpha\beta}$ 'tilt'	$C_{\alpha\beta}$ 'twist'
E1	tilted	potential	$0 < t < \delta t$	$0 < t < \delta t$	1	0
E2	twisted	harmonic	$0 < t < \delta t/3$	$\delta t/3 < t < \delta t$	0	1
E3	twisted-tilted	potential	$0 < t < \delta t/3$	$\delta t/3 < t < \delta t$	1	1
E4	tilted	harmonic	$0 < t < \delta t$	$0 < t < \delta t$	-1	0
E5	tilted	harmonic	$0 < t < \delta t$	$0 < t < \delta t$	1	0
E6	twisted-tilted	harmonic	$0 < t < \delta t$	$0 < t < \delta t$	1	1

NOTE— We set the initial axisymmetric poloidal magnetic field strength to zero. For the runs E5 and E6 we vary the range the BMR's initiation latitude from -40° to 40°. For the run E6 we made the additional run with initiation at 20° latitude and the initial axisymmetric poloidal magnetic field geometry as shown in Figure 1.

For the simultaneous action of $\mathcal{E}_1$ and $\mathcal{E}_2$, in the case E1, we obtain a tilted BMR illustrated in Figure 2. The tilt of the BMR does not change much during emergence in this case. The figure illustrates two other situations. Case E2 employs the boundary conditions of the harmonic magnetic field (Appendix B). In this case, $\mathcal{E}_{\rm I}$ acts during the pre-emergence stage, then it is turned off, and the BMR starts to rise due to the action of $\mathcal{E}_2$. This model run shows the clockwise rotation of 180° of BMR during the emerging phase. Case E6 is the same as E1, but with the harmonic magnetic field boundary conditions. In run E6, the magnetic polarities rotate anticlockwise by approximately 135°. These effects qualitatively correspond to observational results (e.g., Tian et al. 2005; Sturrock et al. 2015; Grigoryev & Ermakova 2025). In both cases, E2 and E6, we find that the polarity pattern is slightly more elongated along the polarity inversion line than in cases E1 and E4.

Using our analytical expressions for the mean electromotive force (Appendix A), we introduce the following definition for the helicity density flux outward of the dynamo region:

$$F_{\Omega} = 2\left\langle B\right\rangle_r \left\langle A\right\rangle_\phi \left\langle U\right\rangle_\phi\,, \tag{19}$$

$$F_U = 2\left\langle B\right\rangle_r \left\langle A\right\rangle_\theta \left\langle U\right\rangle_\theta \,, \tag{20}$$

$$F_r^{\langle ab\rangle} = -\eta_\chi \left(\hat{\mathbf{r}}\cdot\nabla\right)\left\langle \boldsymbol{a}\cdot\boldsymbol{b}\right\rangle \,, \tag{21}$$

where the small-scale helicity density is estimated from Eq. (18). To estimate the effect of the BMR's twist, tilt, and the effect of the turbulent diffusion, we take into account the isotropic structure of the hydrodynamic α-effect and turbulent diffusion near the solar surface. We define the helicity density flux from the mean electromotive force as follows, $F_{\mathcal{E}} = F_{\alpha\beta} + F_\eta$, where $F_{\alpha\beta}$ determines the flux from the magnetic field twist and tilt of the BMR rising from the depth of the convection zone,

$$F_{\alpha\beta} = 2\left(\alpha_{\phi\phi} + \alpha_\beta^{\mathrm{BMR}}\right)\left(\left\langle B\right\rangle_\phi \left\langle A\right\rangle_\theta - \left\langle B\right\rangle_\theta \left\langle A\right\rangle_\phi\right) - 2V_\beta\left(\left\langle B\right\rangle_\theta \left\langle A\right\rangle_\theta + \left\langle B\right\rangle_\phi \left\langle A\right\rangle_\phi\right), \tag{22}$$

where we see that only the horizontal components of the magnetic field and vector potentials contribute to $F_{\alpha\beta}$. The effect of the turbulent diffusion has three contributions:

$$F_\eta = -2\eta_T \hat{\mathbf{r}}\cdot\left(\left\langle\boldsymbol{A}\right\rangle\times\left\langle\boldsymbol{J}\right\rangle\right) = -2\eta_T\left(\hat{\mathbf{r}}\cdot\nabla\right)\left(\left\langle\boldsymbol{A}\right\rangle\cdot\left\langle\boldsymbol{B}\right\rangle\right) + 2\eta_T\left(\left\langle\boldsymbol{A}\right\rangle\cdot\nabla\right)\left\langle B\right\rangle_r + 2\eta_T\left(\left\langle\boldsymbol{B}\right\rangle\cdot\boldsymbol{\nabla}\right)\left\langle A\right\rangle_r \,, \tag{23}$$

where the first term shows the same type of helicity flux as the diffusive flux of turbulent magnetic helicity in Eq. (21).

4. RESULTS

4.1. *Evolution of magnetic helicity fluxes and tilt and twist of emerging BMR*

Figure 3 shows the snapshots of the magnetic field configuration and helicity flux distributions after the BMR emergence for the cases E1, E2, E4, and E5 at the middle stage of the BMR evolution. From these model runs, we see that the magnitude and sign of the helicity flux distribution significantly depends on the boundary conditions, the sign of the tilt, and the mutual phase of the initial perturbations, ξ_1 and ξ_2 in Eq. (16). The runs with the harmonic magnetic field boundary conditions, e.g., E2, E4, and E5, show higher magnitudes of the surface magnetic helicity density and the helicity flux initiated by the α-effect, and magnetic buoyancy, $F_{\alpha\beta}$, than the run E1. Similarly to the analysis of Pariat et al. (2005), we see that the emergence of the BMR induces specific polarity patterns for each mechanism of the magnetic helicity flux. The results for the helicity density flux distributions

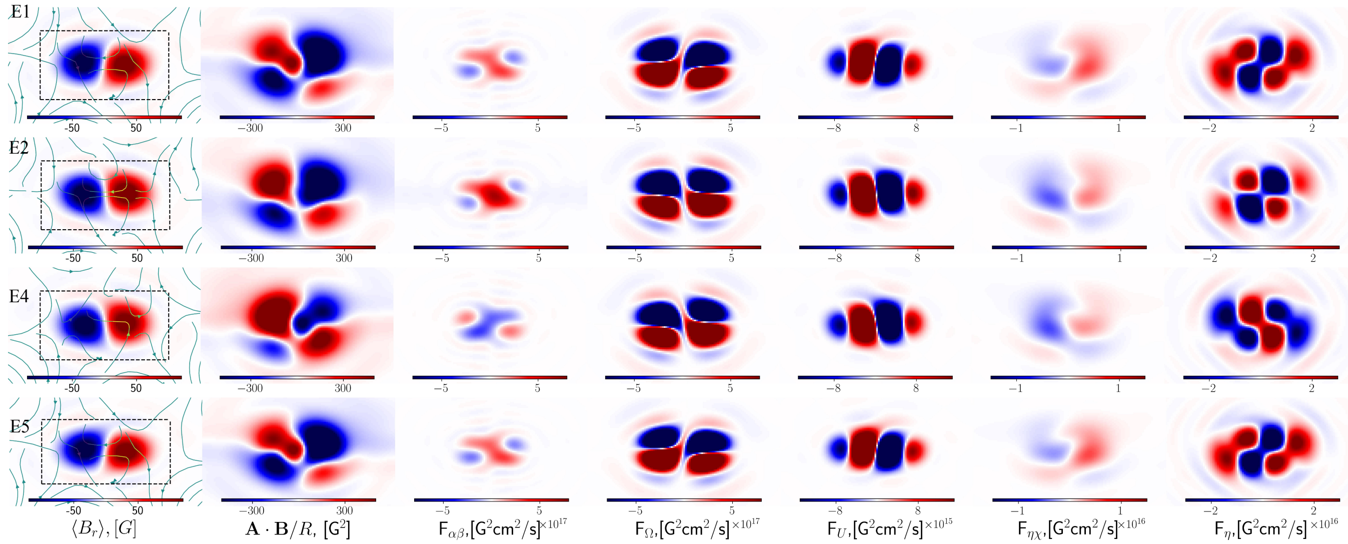

Figure 3. Snapshots of the magnetic field, the magnetic helicity density, and the helicity density fluxes at the middle state of the active region evolution: (a) the surface magnetic field; (b) the total magnetic helicity density, $\boldsymbol{A}\cdot\boldsymbol{B}$; the panels (c), (d), (e) (f) and (g) show the density of the magnetic helicity flux distributions $F_{\alpha\beta}$, F_{Ω}, F_U, $F_{\eta\chi}$, and F_{η}. The rectangle indicates the area used for calculating the BMR helicity flux.

due to the effects of the differential rotation and meridional circulations are qualitatively in agreement with the patterns discussed in the paper mentioned above. Also, we see that the flux, $F_{\alpha\beta}$, which stems from the α-effect and the helicity density initiated by the BMR rise, is similar to the flux from the rotational motions of the magnetic polarities relative to each other (see, Pariat et al. 2005; Yamamoto 2011).

Figure 4 shows the evolution of the integral parameters: the total unsigned radial magnetic field flux, the surface helicity density, the total helicity flux, and the tilt of the BMR, calculated following the procedure accepted in the SHARP routine (Liu et al. 2014; Sun et al. 2024). The total magnetic flux and other integral parameters are calculated in the area marked by the dashed line in Figure 3. Some part of this flux further contributes to the large-scale dynamo in the solar convection zone. It is noteworthy that restricting the area of the integral neglects the effect of the large-scale, nonaxisymmetric magnetic field in the helicity flux. The total helicity flux in cases E2, E4, E5, and E6 sharply increases at the beginning of the BMR emergence because of the helicity transport by the twisted magnetic field rising from the convection zone. At the end of emergence, the largest contribution to the helicity flux is due to the effect of differential rotation. We find that if we integrate the flux over the whole surface, the sharp increase of the flux, which is seen in Figure 4b at the beginning phase of BMR evolution, disappears. This tells about the importance of the large-scale nonaxisymmetric magnetic field contribution to the helicity flux. The BMR's tilt can evolve in a different way, which depends on whether the BMR was twisted before emergence. For example, for case E1, the BMR's tilt decreases continuously until $\approx 5°$ and then it shows some variations about this value caused by the BMR's evolution. The twisted BMRs show the anti-Hale direction of the tilt at the beginning of their emergence.

The surface magnetic helicity density shows sign variations. For all cases, except E4, we find the predominantly negative helicity density of the magnetic field during the model runs. In the case of the negative tilt, case E4, the BMR shows an inversion of the helicity sign from positive to negative at the end of this model run. This is caused by the differential rotation effect. Further results that support this conclusion are shown in Figure 6. The runs, which employ the harmonic boundary conditions, show a positive helicity density at the very beginning of the BMR's emergence.

Figure 5 shows the evolution of the integral parameters of the magnetic helicity flux. The helicity flux rate is higher than the magnetic flux rate. This agrees with the analysis of observations made by Liu et al. (2014); Norton et al. (2023); Sun et al. (2024). The interesting finding is that the helicity flux due to the turbulent diffusion in the radial direction, $F_{\eta V}$, dominates the contribution from the diffusion in the horizontal direction $F_{\eta H}$. In other words, in the expression of the turbulent diffusion helicity flux:

$$F_{\eta} = F_{\eta V} + F_{\eta H}, \tag{24}$$

$$F_{\eta V} = -2\eta_T \nabla \left(\langle \boldsymbol{A} \rangle \cdot \langle \boldsymbol{B} \rangle \right) + 2\eta_T \left(\langle \boldsymbol{B} \rangle \cdot \nabla \right) \langle \boldsymbol{A} \rangle , \tag{25}$$

$$F_{\eta H} = 2\eta_T \left(\langle \boldsymbol{A} \rangle \cdot \boldsymbol{\nabla} \right) \langle \boldsymbol{B} \rangle , \tag{26}$$

we should take the radial components of the fluxes into account. Using the identity $\hat{\mathbf{r}} \cdot \langle \boldsymbol{A} \rangle^{(p)} = 0$, we see that the second term in $F_{\eta V}$ is zero. The contribution $F_{\eta V}$ dominates $F_{\eta H}$. Moreover, because of the condition $\nabla \cdot \langle \mathbf{A} \rangle^{(p)} = 0$, the total surface integral of contribution $F_{\eta H}$ is close to zero. The

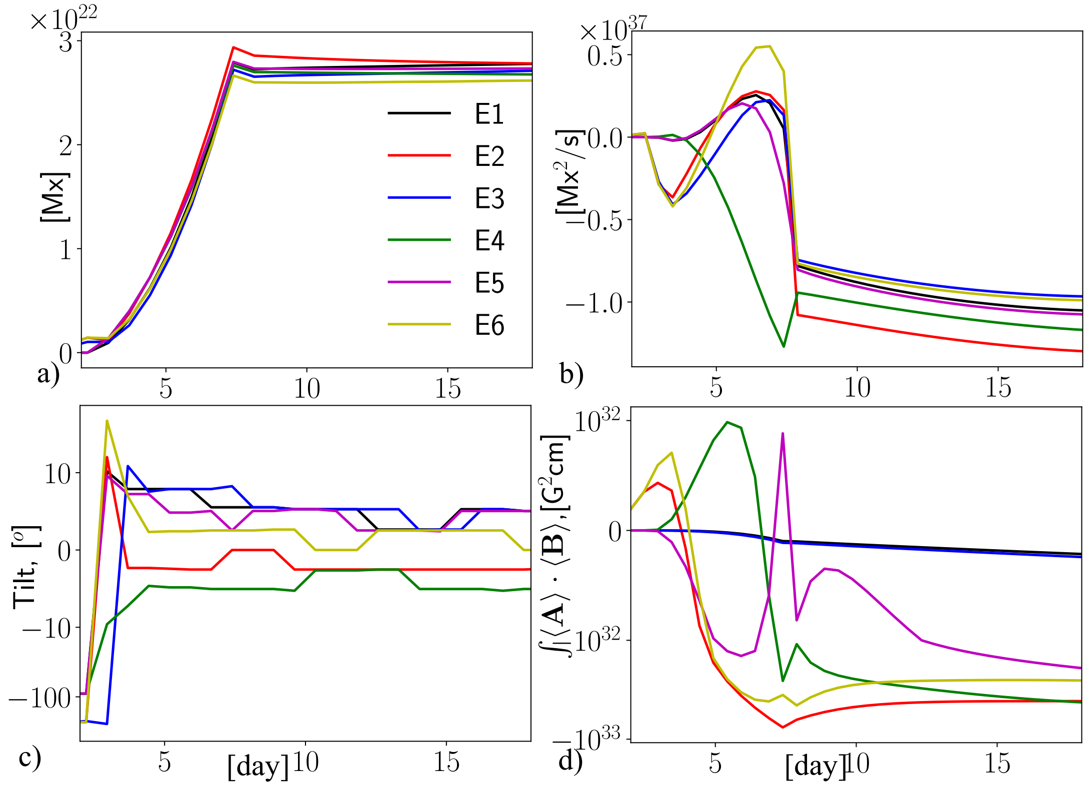

Figure 4. Evolution of the BMR's parameters during emergence: a) the total unsigned radial magnetic field flux on from BMR's area marked by the dash line in Figure 3; b) the total helicity flux from BMR; c) evolution of the BMR's tilt; d) the total surface magnetic helicity density.

comparison of Figures 5(c) and(g) shows that $F_{\eta V}$ is approximately 4 orders of magnitude higher than $F_{\eta H}$.

Comparing Figures 5 (c) and (d), we see that the diffusive decay of the BMR is an order of magnitude larger than the diffusive flux of the small-scale magnetic helicity (Eq. 11). This is because the magnitude of the turbulent diffusion of the magnetic field is by an order of magnitude larger than the turbulent diffusion.

We compute the distributions of the current helicity density $\left\langle \mathbf{B}_{\|}\right\rangle \left(\nabla\times\langle\boldsymbol{B}\rangle\right)_{\|}$ and the total current helicity. Here $\langle\mathbf{B}_{\|}\rangle = \sin\theta\langle B_r\rangle + \cos\theta\langle B_\theta\rangle$ is the line-of-sight magnetic field. For the potential boundary conditions, the radial component of current is zero, $\left(\nabla\times\langle\boldsymbol{B}\rangle\right)_r = 0$. Nevertheless, the projection effects can result in nonzero values of $\left\langle \boldsymbol{B}_{\|}\right\rangle \left(\nabla\times\langle\boldsymbol{B}\rangle\right)_{\|}$. Following Hagino & Sakurai (2004), we calculated the weighted values of the force-free parameter α, using the average over the

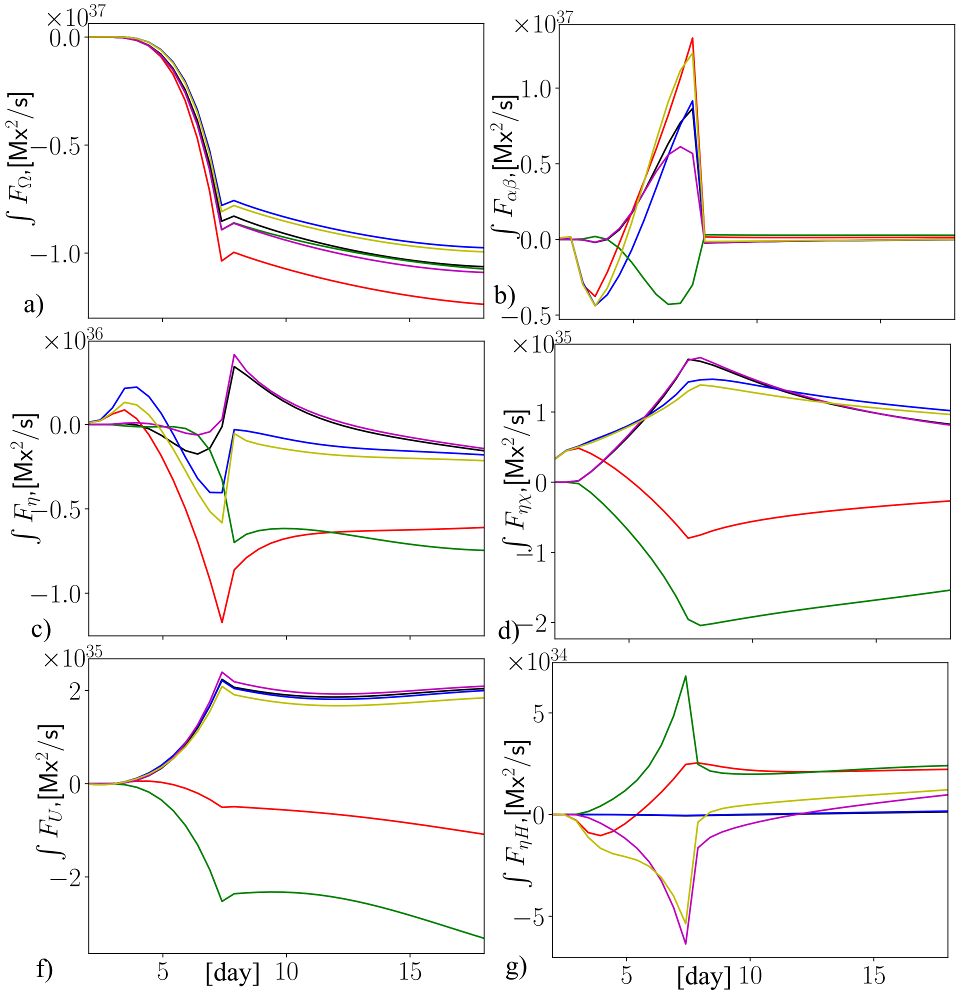

Figure 5. Evolution of the BMR's helicity flux during emergence: a) the evolution of the helicity flux due to the differential rotation, F_{Ω}; b) the helicity flux by the BMRs' tilt/twist, $F_{\alpha\beta}$; c) the flux initiated by BMRs' decay due to the turbulent diffusion, F_{η}; d) the diffusive flux of the small-scale magnetic helicity; e) the helicity flux by the meridional circulation, F_{U}; f) the flux initiated by BMRs' decay due to the horizontal turbulent diffusion, $F_{\eta H}$.

active region amplitudes of the electric currents and magnetic field:

$$\alpha_{\rm av}=\frac{\int\left\langle B_{\parallel}\right\rangle \left(\nabla\times\left\langle \boldsymbol{B}\right\rangle \right)_{\parallel}{\rm d}S}{\int\left\langle B_{\parallel}\right\rangle ^{2}{\rm d}S}, \tag{27}$$

$$\alpha_{\rm ff}=\frac{\int\left\langle \boldsymbol{B}\right\rangle \cdot\left(\nabla\times\left\langle \boldsymbol{B}\right\rangle \right){\rm d}S}{\int\left\langle B\right\rangle ^{2}{\rm d}S}, \tag{28}$$

$$\alpha_{\rm avr}=\frac{\int\left\langle B_{r}\right\rangle \left(\nabla\times\left\langle \boldsymbol{B}\right\rangle \right)_{r}{\rm d}S}{\int\left\langle B_{r}\right\rangle ^{2}{\rm d}S}, \tag{29}$$

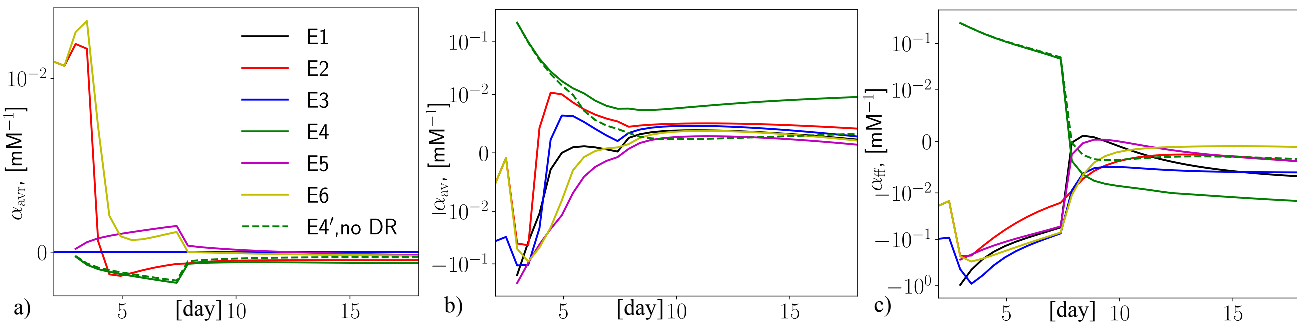

Figure 6. Evolution of the parameters $\alpha_{\rm avr}$ (a), $\alpha_{\rm av}$ (b), and $\alpha_{\rm ff}$ (c). The green dashed line shows results for the run E4′ with the neglected effect of the differential rotation.

Figure 6 shows the results. The maximum amplitude of the twist parameters, α_{avr}, α_{av} and the total twist parameter $\alpha_{\rm ff}$, are by an order of magnitude larger than $\alpha_{\rm best}$ in observations (e.g., Tian et al. 2005; Kuzanyan et al. 2006). The state-of-the convective magnetic flux emergence simulations of Toriumi et al. (2024) for a kink-unstable magnetic tube showed the same magnitude of $\alpha_{\rm ff}$ as in our models. We made the additional run for the setup E4, where we skipped the effect of the differential rotation on the magnetic field evolution (case E4′ in Figure 6). It shows that shortly after emergence (after day 5), the magnitude and sign of α_{av} are determined by the effect of the differential rotation on the meridional component of the magnetic field. The runs with the potential boundary conditions show $\alpha_{\rm ff} \gg \alpha_{\rm av}$ because $\left(\nabla\times\langle\boldsymbol{B}\rangle\right)_r = 0$. This means that in such a situation, the twist of the magnetic field in the horizontal direction dominates the twist in the vertical direction.

4.2. *The hemispheric helicity rule*

We compute the latitudinal variations of the current helicity parameter α_{av} and the total helicity flux to see how well the theoretically studied active regions fit into the hemispheric helicity rule. Figure 7 shows these parameters together with the latitudinal variation of tilt for the E5 and E6 model setups. Model E6 shows an angle of inclination about twice that of the tilt angle profile of model E5. In addition, the scatter of the latitudinal profiles of α_{av} and the total helicity flux is higher in model E6. We find that for these types of active regions, the hemispheric rule changes during evolution. In the final state, the hemispheric rule is determined by the effect of the differential rotation.

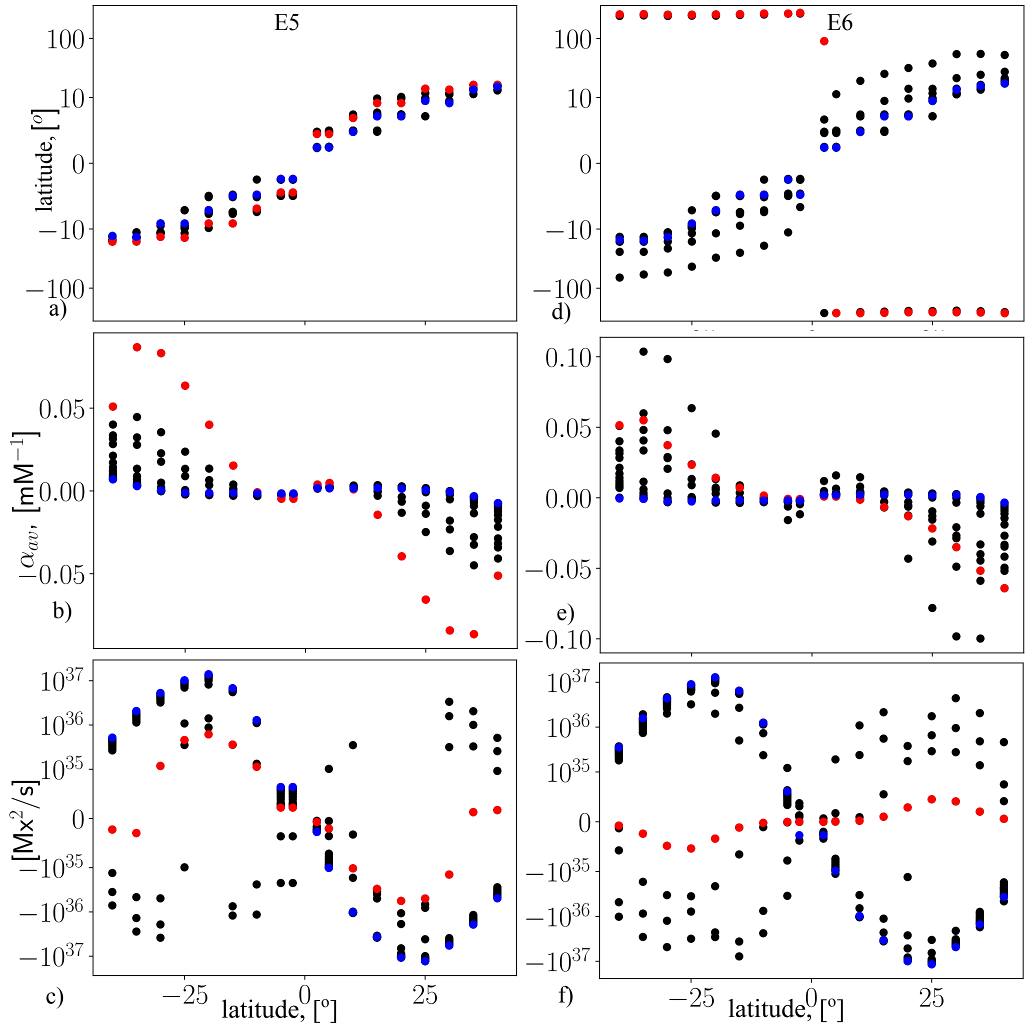

Figure 7. Latitudinal dependence of the tilt (a), the parameter $\alpha_{\rm ff\|}$(b) and the total flux (c) for the model setup E5. The red circles show the value at the beginning of the BMR emergence, and the blue circles show the same for the final stage of the run. The second column with panels d), e), and f) shows the same parameters for the model setup E6. The vertical scale in panel (d) is linear in the range of $\pm 10°$ and logarithmic outside this range.

Using the helicity flux calculations, we compute the total helicity that is transported through the area of the BMRs marked by a rectangle in Figure 3 (Toriumi et al. 2024; Sun et al. 2024),

$$\Delta H = \int \frac{\partial H}{\partial t} \mathrm{d}t \tag{30}$$

The data drawn in Figure 8a show a power-law dependence, $\Delta H \sim 0.02\Phi^2$, where Φ the maximum total flux of the radial magnetic field. The results of Sun et al. (2024) suggested a similar power exponent. Such a value of the power exponent shows that the magnetic field configuration is topologically close to a simple linkage of two close magnetic loops around each other. **In contrast to Sun et al. (2024), our model shows some increase in the linkage parameter with the amount of magnetic flux. This difference is probably because of the different definitions for the helicity flux. The paper of Sun et al. (2024) employs the relative magnetic helicity.**

5. DISCUSSION AND CONCLUSIONS

In this study, we modeled some typical configurations of magnetic bipolar active regions (BMR) using the previously developed 3D non-linear mean-field MHD solar dynamo model, which includes the emergence of BMRs due to a magnetic buoyancy instability (Pipin et al. 2023). In this model, the turbulent hydrodynamic and magnetic helicity (the α-effect), acting locally on the unstable parts of the toroidal magnetic field that form the bipolar active region, produces the twist and tilt of the magnetic field inside the BMRs. We calculated the magnetic helicity flux from the dynamo region to the outer layers initiated by the BMR's emergence. Starting from Fan (2001), similar studies were done previously using simulations of the kink-unstable magnetic flux tube in the convective media in a number of papers (see, e.g.,Prior & Yeates 2014; Prior & MacTaggart 2019; Toriumi & Wang 2019; Toriumi et al. 2024). Similarly to these papers, in our simulations, we did not take into account the non-axisymmetric hydrodynamic motions and heat transport around the BMR. However, the dynamo model describes the non-linear magnetic effects on the axisymmetric flow and the convective heat transport. Our approach to modeling the evolution of the photospheric BMR is rather simple. Nevertheless, this model is a step toward a consistent picture of the large-scale convection zone dynamo describing important parameters of the active regions on the solar surface such as the tilt and twist of the magnetic field.

In the standard surface flux-transport model (hereafter SFT, e.g., Yeates et al. 2023), a solar active region is approximated by a simple bipolar magnetic structure, which is tilted according to Joy's law. In SFT models, the hemispheric helicity rule can result from the differential rotation effect on the surface evolution of BMRs (Prior & Yeates 2014). Hawkes & Yeates (2019) utilized the SFT to estimate the helicity flux initiated by the emergence and evolution of the BMRs. Their expression

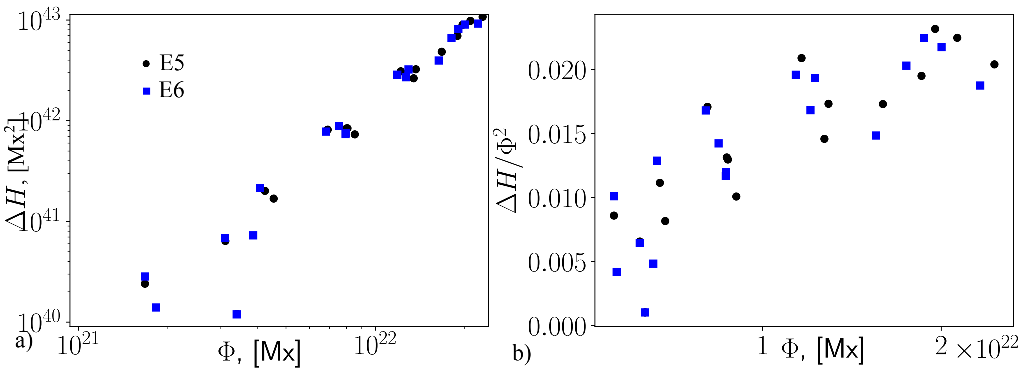

Figure 8. a) The helicity $\Delta H = \int \partial_t H \mathrm{d}t$ accumulated in the BMRs versus the maximum total flux of the radial magnetic field, Φ; the black circles show results for the model setup E5, and blue squares show the same for the model setup E6; b) the same for the normalized value, $\Delta H/\Phi$.

of the helicity flux employs the effects of the global flow, including the differential rotation and meridional circulation, and the effect of the surface turbulent diffusion. The mean-field formalism, which is employed here to model both the large-scale dynamo and the BMRs, allows us to estimate the possible effect of the tilt and twist of the rising active regions on the helicity flux and evolution of the mean twist of the solar active regions. We also take into account the radial structure of the magnetic field below the surface. For the first time, such calculations are performed using a large-scale 3D solar dynamo model, consistent with helioseismic and surface observations (Pipin et al. 2023; Mandal et al. 2024).

We see that the action of the α-effect on the rising part of the large-scale toroidal magnetic field can result in a complicated evolution of the magnetic flux in the emerging BMRs. Similarly to the numerical model of the twisted magnetic tubes subjected to the kink instability (Fan 2001), our model, e.g., the runs E2, E3, and E6, show a rotation of the BMR when the α-effect is applied before the rising stage of the BMR evolution. Rotation of BMRs is often observed in the evolution of the solar active regions (Tian et al. 2005).

The model shows a monotonic increase in the magnetic flux before the end of the emerging stage. The helicity flux can grow sharply at the beginning because of the rise of the twisted magnetic field. This agrees with the results of the observations of Liu et al. (2014); Sun et al. (2024) and with the state-of-the-art model of Toriumi et al. (2024). Similarly to the observational results, we find that at the end of the BMR evolution, the major effect in the helicity flux is due to the differential rotation. Another interesting finding is that our model shows a significant helicity flux induced by the radial gradient of the magnetic helicity of the BMRs. This flux was theoretically suggested by Mitra et al. (2011); Kleeorin & Rogachevskii (2022); Gopalakrishnan & Subramanian (2023). The mean-field models showed that it can significantly affect the dynamo solution (Guerrero et al. 2010). Here, we calculated this contribution to the helicity flux for the BMR. We plan to study its effect on the dynamo cycles in our future studies.

The model shows that, unlike the magnetic helicity flux, the twist parameters, such as α_{avr} and α_{av} (Eqs 27−29) can develop quickly during the initial phase of BMR emergence. This reflects both the effect of the current preexisting before the magnetic field emerges at the surface and the evolution of the magnetic field topology inside the BMR during the rising phase. In our model, the result of this evolution depends on the initial and surface boundary conditions. In observations (e.g., Leka et al. 1996), this behavior is often interpreted as a sign that the magnetic field is twisted before it emerges. In runs E2 and E6 (Table 1), the initial positive sign of α_{avr} and α_{av} corresponds to the sign of the mean electromotive force applied to the toroidal magnetic field before the BMR rise. These parameters quickly change to negative (Figure 4b) because of the dynamic response of the magnetic configuration to the conservation of total magnetic helicity. This result is consistent with interpretations of the helicity of the solar active regions suggested by the mean-field dynamo models (Sokoloff et al. 2006). Yet, our results show that after the BMR emergence, the helicity of the solar active regions is quickly modified by the effect of the differential rotation. In the final stage, the BMR's twist parameter α_{av} shows the hemispheric helicity rule. In the model, the small magnitude of twist is supported by the effect of differential rotation. It is noteworthy that the hemispheric helicity rule can depend on the phase of the magnetic cycle (e.g., Zhang et al. 2010). Here, we do not consider this effect. The helicity flux shows the hemispheric helicity rule as well. Our results agree with the results of Berger & Ruzmaikin (2000) and Hawkes & Yeates (2019) in this regard.

In this paper, we discussed the helicity flux from the dynamo region into the corona caused by the BMR's emergence. Injection of the BMRs also has to produce fluxes

in the latitudinal direction. Such fluxes can affect the parity of the dynamo solution (Mitra et al. 2010). We postpone discussion of this effect to another study.

Let us summarize our findings. Using the mean-field MHD formalism, we estimated the influence of BMR's tilt and twist on the helicity flux. Our model shows that the action of the α-effect before and during the BMR emergence results in a complex evolution of magnetic configuration, affecting variations of the twist and tilt of the emergent BMR. Such variations are caused by the magnetic helicity conservation, large-scale flows, and turbulent diffusion of the magnetic field. The findings highlight the differential rotation as a key driver of helicity flux, with significant effects induced by radial magnetic helicity gradients. While the twist parameters evolve quickly during the BMR emergence, influenced by initial and surface conditions, the differential rotation strongly impacts helicity flux consistency with the hemispheric helicity rule. We conclude that BMR twists and helicity quickly adapt to the post-emergence state. Further research is needed to understand the impacts of active region helicity fluxes on the dynamo cycles.

Acknowledgments: Resources supporting this work were provided by the NASA High-End Computing (HEC) Program through the NASA Advanced Supercomputing (NAS) Division at Ames Research Center. This work is supported by the Chinese Academy of Sciences (CAS) President's International Fellowship Initiative (PIFI) No 2024PVA0093. In addition, VP thanks the financial support of the Ministry of Science and Higher Education (subsidy No.075-GZ/C3569/278).

APPENDIX

A. MAGNETIC HELICITY BUDGET IN THE DYNAMO MODEL.

The details of our model can be found in the paper of Pipin et al. (2023). Here, we review the parts of the model that are directly related to the subject of the paper.

The dynamo model employs the mean electromotive force, $\boldsymbol{\mathcal{E}}$, as follows.

$$\mathcal{E}_i = \left(\alpha_{ij} + \gamma_{ij}\right) \left\langle B \right\rangle_j - \eta_{ijk} \nabla_j \left\langle B \right\rangle_k + \mathcal{E}_i^{(\mathrm{BMR})}, \tag{A1}$$

where $\boldsymbol{\mathcal{E}}^{(\mathrm{BMR})}$ represents the contribution, which prescribes the generation of the bipolar active regions, α_{ij} describes the turbulent generation by the hydrodynamic and magnetic helicity, γ_{ij} is the turbulent pumping and η_{ijk} - the eddy magnetic diffusivity tensor. In particular, the α-effect tensor includes the effect of magnetic helicity conservation (Kleeorin & Ruzmaikin 1982; Kleeorin & Rogachevskii 1999),

$$\alpha_{ij} = C_{\alpha}\psi_{\alpha}(\beta)\alpha_{ij}^{\mathrm{K}} + \alpha_{ij}^{\mathrm{M}}\psi_{\alpha}(\beta)\frac{\langle\mathbf{a}\cdot\mathbf{b}\rangle\,\tau_c}{4\pi\overline{\rho}\ell_c^2}. \tag{A2}$$

Here C_{α} is the dynamo parameter characterizing the magnitude of the hydrodynamic α-effect, and α_{ij}^{K} and α_{ij}^{M} describe the anisotropic properties of the kinetic and magnetic α-effect (Pipin 2008; Pipin & Kosovichev 2019; Brandenburg et al. 2023). The radial profiles of α_{ij}^{H} and α_{ij}^{M} depend on the mean density stratification and the spatial profiles of the convective velocity u_c, and on the Coriolis number,

$$\mathrm{Co} = 2\Omega_0\tau_c, \tag{A3}$$

where Ω_0 is the global angular velocity of the star, and τ_c is the convective turnover time. The magnetic quenching function $\psi_{\alpha}(\beta)$ depends on the parameter $\beta = |\langle\mathbf{B}\rangle|/\sqrt{4\pi\overline{\rho}u_c^2}$ (Pipin & Kosovichev 2019). We used the analytical expressions of the coefficients of $\boldsymbol{\mathcal{E}}$ given by Pipin (2008). The initiation of the bipolar magnetic regions is determined by $\mathcal{E}_i^{(\mathrm{BMR})}$, see Section 3 and for more details in Pipin et al. (2023):

$$\boldsymbol{\mathcal{E}}^{(\mathrm{BMR})} = \alpha_{\beta}^{\mathrm{BMR}}\left\langle\boldsymbol{B}\right\rangle + V_{\beta}\left(\hat{\boldsymbol{r}}\times\langle\mathbf{B}\rangle\right), \tag{A4}$$

where the first term takes into account the BMR's tilt/twist and the second term models the emergence of the surface magnetic region in the bipolar form. The induction equation (Eq. 12) describes the evolution of both the large-scale magnetic field and the evolution of the BMRs. **It is noteworthy that the longitudinal averaging of $\boldsymbol{\mathcal{E}}^{(\mathrm{BMR})}$ results in the additional generation effect of the large-scale axisymmetric magnetic field and the additional sources of the magnetic flux loss Pipin (2022). Therefore, the critical threshold of the mean field parameter C_{α} decreases in the presence of $\boldsymbol{\mathcal{E}}^{(\mathrm{BMR})}$. Presumably, the mean-field dynamo can operate with the BMR electromotive force $\boldsymbol{\mathcal{E}}^{(\mathrm{BMR})}$ alone, starting from a quite large amount of**

toroidal magnetic flux inside the convection zone, i.e., due to the non-linear dynamo instability (Ferriz-Mas et al. 1994). Such dynamo instability can depend on the parameters of the BMR's injection functions, see Appendix C. However, we have not studied this issue.

Uncurling the induction equation for $\langle \boldsymbol{B} \rangle$, we obtain the evolution equation for the mean vector-potential,

$$\frac{\partial \langle \boldsymbol{A} \rangle}{\partial t} = (\boldsymbol{\mathcal{E}} + \langle \boldsymbol{U} \rangle \times \langle \boldsymbol{B} \rangle) + \boldsymbol{\nabla} h, \tag{A5}$$

where h is an arbitrary scalar function.

Before proceeding further, we discuss the problem of the gauge. We decompose the large-scale magnetic field and flows into the sum of axisymmetric and nonaxisymmetric parts:

$$\begin{aligned} \langle \boldsymbol{B} \rangle &= \langle \overline{\boldsymbol{B}} \rangle + \left\langle \tilde{\boldsymbol{B}} \right\rangle, \\ \langle \boldsymbol{A} \rangle &= \langle \overline{\boldsymbol{A}} \rangle + \left\langle \tilde{\boldsymbol{A}} \right\rangle, \end{aligned}$$

Moreover, the nonaxisymmetric part is decomposed into a sum of the poloidal and toroidal superpotentials:

$$\left\langle \tilde{\boldsymbol{B}} \right\rangle = \nabla \times \boldsymbol{r} \tilde{T}(\boldsymbol{r}, t) + \nabla \times \nabla \times \boldsymbol{r} \tilde{S}(\boldsymbol{r}, t), \tag{A6}$$

where $\boldsymbol{r}$ is the radius vector in the spherical coordinate system; $\tilde{S}$ and $\tilde{T}$ are the scalar potentials(Krause & Rädler 1980). It is noteworthy that the axisymmetric field can be decomposed into the sum of the poloidal and toroidal parts as well:

$$\langle \overline{\boldsymbol{B}} \rangle = B \boldsymbol{e}_{\phi} + \nabla \times \left(\frac{A \boldsymbol{e}_{\phi}}{r \sin \theta} \right) \tag{A7}$$

where the scalars B and A are the functions of time, r is the radius, θ is the co-latitude (the polar angle), and $\boldsymbol{e}_{\phi}$ is the unit vector along the azimuth. In our notations, we can write,

$$\begin{aligned} \langle \overline{\boldsymbol{A}} \rangle &\equiv \frac{A}{r \sin \theta} \boldsymbol{e}_{\phi} \\ \left\langle \tilde{\boldsymbol{A}} \right\rangle &= \boldsymbol{r} \tilde{T}(\boldsymbol{r}, t) + \nabla \times \boldsymbol{r} \tilde{S}(\boldsymbol{r}, t) + \boldsymbol{\nabla} g, \end{aligned}$$

Following Krause & Rädler (1980), we note that the arbitrarily chosen scalar h is a function of the radial coordinate, r, and the same is true for g. This uncertainty can be removed if we consider the integrals of the scalars $\tilde{T}$ and $\tilde{S}$ over the solid angle normalized to zero, i.e. $\int_0^{2\pi}\int_{-1}^{1}\tilde{S}\mathrm{d}\mu\mathrm{d}\phi = \int_0^{2\pi}\int_{-1}^{1}\tilde{T}\mathrm{d}\mu\mathrm{d}\phi = 0$, where $\mu = \cos\theta$. This gauge is valid by default for $\left\langle\overline{\boldsymbol{A}}\right\rangle$ because it satisfies the Coulomb gauge, $\boldsymbol{\nabla}\cdot\left\langle\overline{\boldsymbol{A}}\right\rangle \equiv 0$. Assuming the above normalization procedure and decompositions of the large-scale field given by Equations (A6) and (A7), we can omit the contribution $\boldsymbol{\nabla}h$ from the equation for the mean vector-potential evolution. After some algebra, we get the evolution equation for the helicity density of the mean magnetic field,

$$\frac{\partial\left\langle\boldsymbol{A}\right\rangle\cdot\left\langle\boldsymbol{B}\right\rangle}{\partial\mathrm{t}}+\boldsymbol{\nabla}\cdot\left(\left\langle\boldsymbol{U}\right\rangle\left\langle\boldsymbol{A}\right\rangle\cdot\left\langle\boldsymbol{B}\right\rangle\right)=2\boldsymbol{\mathcal{E}}\cdot\left\langle\boldsymbol{B}\right\rangle+2\nabla\cdot\left(\boldsymbol{\mathcal{E}}\times\left\langle\boldsymbol{A}\right\rangle\right) \tag{A8}$$

$$+2\nabla\cdot\left\langle\boldsymbol{B}\right\rangle\left(\left\langle\boldsymbol{A}\right\rangle\cdot\left\langle\boldsymbol{U}\right\rangle\right)-\nabla\cdot\left\langle\boldsymbol{U}\right\rangle\left(\left\langle\boldsymbol{A}\right\rangle\cdot\left\langle\boldsymbol{B}\right\rangle\right)$$

$$-2\eta\left\langle\boldsymbol{B}\right\rangle\cdot\left\langle\boldsymbol{J}\right\rangle+\nabla\cdot\left(2\eta\left\langle\boldsymbol{A}\right\rangle\times\left\langle\boldsymbol{J}\right\rangle+\left\langle\boldsymbol{A}\right\rangle\times\frac{\partial\left\langle\boldsymbol{A}\right\rangle}{\partial t}\right) \tag{A9}$$

where we use the following identities

$$\frac{\partial\left\langle\boldsymbol{A}\right\rangle\cdot\left\langle\boldsymbol{B}\right\rangle}{\partial t}=\left\langle\boldsymbol{A}\right\rangle\cdot\frac{\partial\left\langle\boldsymbol{B}\right\rangle}{\partial t}+\nabla\times\left\langle\boldsymbol{A}\right\rangle\cdot\frac{\partial\left\langle\boldsymbol{A}\right\rangle}{\partial t}=2\left\langle\boldsymbol{A}\right\rangle\cdot\frac{\partial\left\langle\boldsymbol{B}\right\rangle}{\partial t}+\nabla\cdot\left(\left\langle\boldsymbol{A}\right\rangle\times\frac{\partial\left\langle\boldsymbol{A}\right\rangle}{\partial t}\right), \tag{A10}$$

Subtracting Equation (A8) from the total magnetic helicity balance equation (Eq. 10), we get

$$\frac{\mathrm{d}}{\mathrm{d}t}\int\left\langle\boldsymbol{a}\boldsymbol{\cdot}\boldsymbol{b}\right\rangle dV = -2\int\left(\boldsymbol{\mathcal{E}}\cdot\left\langle\boldsymbol{B}\right\rangle\right)dV-\int\frac{\left\langle\boldsymbol{a}\boldsymbol{\cdot}\boldsymbol{b}\right\rangle}{R_m\tau_c}dV \tag{A11}$$

$$-\oint d\boldsymbol{S}\cdot\boldsymbol{F}^{\langle ab\rangle}+\oint d\boldsymbol{S}\cdot\left\langle\boldsymbol{U}\right\rangle\left(\left\langle\boldsymbol{A}\right\rangle\cdot\left\langle\boldsymbol{B}\right\rangle\right)$$

$$-2\oint d\boldsymbol{S}\cdot\left(\boldsymbol{\mathcal{E}}\times\left\langle\boldsymbol{A}\right\rangle\right)-2\oint d\boldsymbol{S}\cdot\left\langle\boldsymbol{B}\right\rangle\left(\left\langle\boldsymbol{A}\right\rangle\cdot\left\langle\boldsymbol{U}\right\rangle\right).$$

Its differential form reads

$$\frac{\mathrm{d}}{\mathrm{d}t}\left\langle\boldsymbol{a}\boldsymbol{\cdot}\boldsymbol{b}\right\rangle=-2\boldsymbol{\mathcal{E}}\cdot\left\langle\boldsymbol{B}\right\rangle-\frac{\left\langle\boldsymbol{a}\boldsymbol{\cdot}\boldsymbol{b}\right\rangle}{R_m\tau_c}-\nabla\cdot\boldsymbol{F}^{\langle ab\rangle}+\nabla\cdot\left\langle\boldsymbol{U}\right\rangle\left(\left\langle\boldsymbol{A}\right\rangle\cdot\left\langle\boldsymbol{B}\right\rangle\right) \tag{A12}$$

$$-2\nabla\cdot\left(\boldsymbol{\mathcal{E}}\times\left\langle\boldsymbol{A}\right\rangle\right)-2\nabla\cdot\left\langle\boldsymbol{B}\right\rangle\left(\left\langle\boldsymbol{A}\right\rangle\cdot\left\langle\boldsymbol{U}\right\rangle\right).$$

This equation shows that the large-scale dynamo produces the magnetic helicity in the bulk of the convection zone by means of the turbulent electromotive force, i.e., due to the source term $-\left(\boldsymbol{\mathcal{E}}\cdot\left\langle\boldsymbol{B}\right\rangle\right)$. This term potentially leads to the so-called catastrophic quenching problem because of the magnetic helicity contribution to the α-effect (Frisch et al. 1975). The other terms of Equation (A12) describe the decay of the magnetic helicity due to the microscopic diffusion and the helicity fluxes because of the turbulent processes, i.e., $\boldsymbol{F}^{\langle ab\rangle}$, and due to effects of the large-scale dynamo evolution. From previous studies, we know that the turbulent fluxes of the small-scale magnetic helicity alleviate the catastrophic quenching of the α-effect.

To calculate the helicity fluxes at the top of the dynamo domain, we employ the isotropic expression for the turbulent diffusion, i.e., $\eta_{ijk} = \eta_T \varepsilon_{ijk} \nabla_j$, where ε_{ijk} is fully antisymmetric Levi-Chevita symbol, and for the *alpha* effect as well. For presentation, we denote the different contributions of the helicity flux density as follows:

$$F_H = F_\Omega + F_U + F^{\langle ab\rangle} + F_{\mathcal{E}}, \tag{A13}$$

and further decompose $F_{\mathcal{E}} = F_{\alpha\beta} + F_\eta$, where

$$F_\Omega = 2\left\langle \boldsymbol{B}\right\rangle_r \left\langle \boldsymbol{A}\right\rangle_\phi \left\langle \boldsymbol{U}\right\rangle_\phi, \tag{A14}$$

$$F_U = 2\left\langle \boldsymbol{B}\right\rangle_r \left\langle \boldsymbol{A}\right\rangle_\theta \left\langle \boldsymbol{U}\right\rangle_\theta, \tag{A15}$$

$$F_r^{\langle ab\rangle} = -\eta_\chi \nabla_r \left\langle \boldsymbol{a}\cdot\boldsymbol{b}\right\rangle, \tag{A16}$$

$$F_{\alpha\beta} = 2\left(\alpha_{\phi\phi} + \alpha_\beta^{\mathrm{BMR}}\right)\left(\left\langle B_\phi\right\rangle\left\langle A_\theta\right\rangle - \left\langle B_\theta\right\rangle\left\langle A_\phi\right\rangle\right) - 2V_\beta\left(\left\langle B_\theta\right\rangle\left\langle A_\theta\right\rangle + \left\langle B_\phi\right\rangle\left\langle A_\phi\right\rangle\right) \tag{A17}$$

$$\begin{aligned} F_\eta &= -2\eta_T\left(\left\langle \boldsymbol{A}\right\rangle \times \nabla \times \left\langle \boldsymbol{B}\right\rangle\right) \qquad \text{(A18)} \\ &= -2\eta_T \nabla\left(\left\langle \boldsymbol{A}\right\rangle \cdot \left\langle \boldsymbol{B}\right\rangle\right) + 2\eta_T\left(\left\langle \boldsymbol{A}\right\rangle \cdot \nabla\right)\left\langle B_r\right\rangle + 2\eta_T\left(\left\langle \boldsymbol{B}\right\rangle \cdot \nabla\right)\left\langle A\right\rangle_r, \end{aligned}$$

where we take into account the isotropic structure of the hydrodynamic α-effect and turbulent diffusion near the solar surface. Here, we see that the turbulent diffusion of the dynamo-generated magnetic field, including the bipolar active regions, produces the same type of helicity flux as the diffusive flux of the turbulent magnetic helicity, $\boldsymbol{F}^{\langle ab\rangle} = -\eta_\chi \boldsymbol{\nabla}\left\langle \boldsymbol{a}\cdot\boldsymbol{b}\right\rangle$. The part of F_η , i.e., $2\eta_T\left(\left\langle \boldsymbol{A}\right\rangle \cdot \nabla\right)\left\langle \boldsymbol{B}\right\rangle$ was included in the study of Hawkes & Yeates (2019). However, the term $2\eta_T \nabla\left(\left\langle \boldsymbol{A}\right\rangle \cdot \left\langle \boldsymbol{B}\right\rangle\right)$ is much larger by magnitude, see Fig.5. Also, in our study, we assume $\hat{\boldsymbol{r}} \cdot \mathrm{d}S = \mathrm{d}\boldsymbol{S}$. Therefore, the change rate of the magnetic helicity is related to the helicity change inside the dynamo domain (Berger & Ruzmaikin 2000).

B. BOUNDARY CONDITIONS

In the solar dynamo models, it is common to employ the vacuum (potential field) boundary conditions at the top Krause & Rädler (1980). Therefore, in this case, we have $\left\langle\overline{B}_{\phi}\right\rangle=0$, $\tilde{T}=0$ at the top, the vector-potential is $\langle\boldsymbol{A}\rangle\equiv\langle\boldsymbol{A}\rangle^{(p)}$, where $\langle\boldsymbol{A}\rangle^{(p)}$ is the vector-potential of the potential part of the magnetic field. It satisfies the conditions $\hat{\mathbf{r}}\cdot\langle\boldsymbol{A}\rangle^{(p)}=0$, and $\nabla\cdot\langle\mathbf{A}\rangle^{(p)}=0$, at the top boundary. For such boundary conditions, the contribution of the helicity flux that stems from the twist and tilt magnetic field of BMRs, $F_{\alpha\beta}\approx0$. It is noteworthy that in the axisymmetric part of the vector potential $\left\langle\overline{\boldsymbol{A}}\right\rangle_{\theta}=0$. Therefore, in the axisymmetric dynamo, the only components of the helicity flux are due to the turbulent diffusion, $\overline{F}_{\eta}=\eta_{T}\frac{\left\langle\overline{A}_{\phi}\right\rangle}{r}\frac{\partial r\left\langle\overline{B}_{\phi}\right\rangle}{\partial r}$ and due to the differential rotation, F_{Ω}. Nevertheless, the impact of this flux on the outer layer is zero because the helicity of the modeled external magnetic field is zero. The same is true when we employ a boundary condition for the penetration of the toroidal magnetic field to the top, e.g., like in the dynamo model of Pipin & Kosovichev (2024). The consistent study of the helicity flux requires including the coronal magnetic field and stellar wind in the dynamo simulations, e.g., similar to simulations of Warnecke et al. (2011); Jakab & Brandenburg (2021); Perri et al. (2021).

The less computationally expensive solution can be to consider the harmonic magnetic field approximation for the outer magnetic field (Bonanno 2016), i.e.,

$$\left(\nabla^{2}+k^{2}\right)\langle\boldsymbol{B}\rangle=0, \tag{B19}$$

for the region $r_t<r<2.5R$ and the radial magnetic field for $r\geq2.5R$. We use $kR=0.1$ as suggested by the results of the above-cited paper. To connect the external magnetic field with the dynamo region, we employ the continuity of the normal component of the magnetic field and the tangential component of the mean electromotive force. For this boundary condition, the continuity of the tangential component of the mean electromotive force determines the magnitude of the toroidal magnetic field at the surface. For the axisymmetric vector potential outside the dynamo domain, we seek a solution in the form of the decomposition of a product of the spherical Bessel functions and associated

Legendre polynomials as follows (cf Bonanno 2016),

$$A\left(x,\theta,t\right)=\sum A^{(n)}\left(t\right)\frac{\left(\gamma^{(n)}j_{n}\left(x\xi\right)+y_{n}\left(x\xi\right)\right)}{\left(\gamma^{(n)}j_{n}\left(x_{e}\xi\right)+y_{n}\left(x_{e}\xi\right)\right)}\sin\theta P_{n}^{1}\left(\theta\right), \tag{B20}$$

where $x=r/R$, $\xi=kR$ and $x_{e}=0.99$ is the external boundary of the dynamo domain; the constants $A^{(n)}\left(t\right)$ and $\gamma^{(n)}$ are determined by the condition of continuity of the radial magnetic field at x_{e}:

$$\frac{\partial A}{\partial x}=\sum\sin\theta P_{n}^{1}\left(\theta\right)A^{(n)}\left(t\right)\left(\frac{n}{x_{e}}-\xi\frac{\left(\gamma^{(n)}j_{n+1}\left(x_{e}\xi\right)+y_{n+1}\left(x_{e}\xi\right)\right)}{\left(\gamma^{(n)}j_{n}\left(x_{e}\xi\right)+y_{n}\left(x_{e}\xi\right)\right)}\right), \tag{B21}$$

and the coronal magnetic field boundary condition, for instance, the pure radial magnetic field at the radius of the source surface. We put this point at $x_{s}=2.5$, where we define $\gamma^{(n)}$:

$$\frac{n}{x_{s}}-\xi\frac{\left(\gamma^{(n)}j_{n+1}\left(x_{s}\xi\right)+y_{n+1}\left(x_{s}\xi\right)\right)}{\left(\gamma^{(n)}j_{n}\left(x_{e}\xi\right)+y_{n}\left(x_{e}\xi\right)\right)}=0.$$

For the axisymmetric toroidal component, the external magnetic field decomposition is similar to Eq(B20):

$$B\left(x,\theta,t\right)=\sum B^{(n)}\left(t\right)\frac{\left(\zeta^{(n)}j_{n}\left(x\xi\right)+y_{n}\left(x\xi\right)\right)}{\left(\zeta^{(n)}j_{n}\left(x_{e}\xi\right)+y_{n}\left(x_{e}\xi\right)\right)}P_{n}^{1}\left(\theta\right), \tag{B22}$$

where $\zeta^{(n)}$ is deduced from the condition at x_{s}, $B\left(x_{s},\theta,t\right)=0$. At the top of the dynamo domain, we require continuity of $\left[\mathcal{E}_{\theta}\right]_{x=x_{e}}=0$ and the same for the toroidal magnetic field. This results in the following boundary condition

$$\eta_{T}\frac{\partial xB}{\partial x}=\eta_{T}^{(+)}\sum P_{n}^{1}\left(\theta\right)B^{(n)}\left(t\right)\left(\left(n+1\right)-\xi x_{e}\frac{\left(\zeta^{(n)}j_{n+1}\left(x_{e}\xi\right)+y_{n+1}\left(x_{e}\xi\right)\right)}{\left(\zeta^{(n)}j_{n}\left(x_{e}\xi\right)+y_{n}\left(x_{e}\xi\right)\right)}\right), \tag{B23}$$

where $\eta_{T}^{(+)}$ is the effective turbulent diffusion in the corona surrounding the dynamo domain. For the case $\eta_{T}^{+}\gg\eta_{T}$ and $\xi,k=0$, we return to the case of the vacuum boundary conditions. Bonanno (2016) considered the case $\eta_{T}^{+}=\eta_{T}$ for the advection-dominated dynamo regime with the α effect concentrated near the bottom of the convection zone. In our model, the turbulent generation is distributed over the bulk of the convection zone. For the case $\eta_{T}^{+}=\eta_{T}$, our model shows a strong surface toroidal magnetic field

of about 200 G magnitude. Solar observations show that in Solar Cycle 24 the surface axisymmetric toroidal magnetic field was about 1 G (Vidotto et al. 2018). The model runs in this paper employ the ratio $\eta_T^+/\eta_T = 200$, which results in the magnitude of the surface toroidal magnetic field about 10 G. Additional studies show that the ratio η_T^+/η_T affects the dynamo instability threshold for the α effect, and the increase of η_T^+/η_T shifts the dynamo threshold close to the model with the vacuum boundary condition. We hope to publish the results of that study separately. The boundary conditions for the superpotentials $\tilde{S}$ and $\tilde{T}$ are considered in the same way as for the axisymmetric magnetic field components.

C. BMR GENERATION FUNCTIONS

.

The functions $\xi_{1,2}$ determine the spatial-temporal properties of the emergence of the BMR. They are defined in the same way as Pipin et al. (2023):

$$\begin{aligned}\xi_{1,2}\left(\boldsymbol{r},t,t_{1,2}\right)= & C_{\beta}\tanh\left(\frac{\mathrm{t}}{\tau_{0}}\right)\exp\left(-m_{\beta}\left(\sin^{2}\left(\frac{\phi-\phi_{m}}{2}\right)\right.\right.\\ & \left.\left.+\sin^{2}\left(\frac{\theta-\theta_{\mathrm{m}}}{2}\right)\right)\right)\psi(r,r_{m},d_{1,2}),\,0<t<t_{1}\vee t_{1}<t<\delta t\\ = & 0,\,t>t_{1}\vee t_{2}>\delta t\end{aligned} \tag{C24}$$

where ψ is a kink-type function of radius,

$$\psi(r,r_{m},d)=\frac{1}{4}\left(1+\mathrm{erf}\left(100\frac{(r-r_{m})}{R}\right)\right) \tag{C25}$$

$$\times\left(1-\mathrm{erf}\left(100\frac{(r-(r_{m}+d))}{R}\right)\right), \tag{C26}$$

where r_m and θ_m are the radius and the co-latitude of the BMR's initiations in the convection zone. We set, $t_1 = \delta t/3$, where $\delta t = 5$ days and the emergence rate $\tau_0 = 1$ day. For the two-stage process, the emergence time will be $\frac{2}{3}\delta t = 4$ days; this corresponds roughly to the emergence parameters of the large solar active regions (Norton et al. 2023). The parameter C_β controls the magnitude of the magnetic flux inside BMR; for $C_\beta = 250$, we get the simulated BMR's flux of $4 \cdot 10^{22}$ Mx, when the original toroidal magnetic field at r_m and θ_m is of the strength 1.5 kG. For the source of the initiation of BMR, we take the toroidal magnetic field in the upper part of the convection zone at the growing stage of the dynamo cycle, where the condition for the magnetic buoyancy instability is satisfied (Pipin et al. 2023).

REFERENCES

Abramenko, V. I., Suleymanova, R. A., & Zhukova, A. V. 2023, MNRAS, 518, 4746, doi: 10.1093/mnras/stac3338

Bao, S., & Zhang, H. 1998, ApJ, 496, L43, doi: 10.1086/311232

Berger, M. A., & Hornig, G. 2018, Journal of Physics A Mathematical General, 51, 495501, doi: 10.1088/1751-8121/aaea88

Berger, M. A., & Ruzmaikin, A. 2000, J. Geophys. Res., 105, 10481, doi: 10.1029/1999JA900392

Blackman, E. G., & Brandenburg, A. 2003, ApJL, 584, L99, doi: 10.1086/368374

Bonanno, A. 2016, ApJL, 833, L22, doi: 10.3847/2041-8213/833/2/L22

Bourdin, P., Singh, N. K., & Brandenburg, A. 2018, ApJ, 869, 2, doi: 10.3847/1538-4357/aae97a

Brandenburg, A. 2018, Astron. Nachr., 339, 631, doi: 10.1002/asna.201913604

Brandenburg, A., Elstner, D., Masada, Y., & Pipin, V. 2023, SSRv, 219, 55, doi: 10.1007/s11214-023-00999-3

Brandenburg, A., & Subramanian, K. 2005, PhR, 417, 1, doi: 10.1016/j.physrep.2005.06.005

Brandenburg, A., Subramanian, K., Balogh, A., & Goldstein, M. L. 2011, ApJ, 734, 9, doi: 10.1088/0004-637X/734/1/9

Chandrasekhar, S., & Kendall, P. C. 1957, ApJ, 126, 457, doi: 10.1086/146413

Choudhuri, A. R. 1992, A&A, 253, 277

Del Sordo, F., Guerrero, G., & Brandenburg, A. 2013, MNRAS, 429, 1686, doi: 10.1093/mnras/sts398

Fan, Y. 2001, ApJL, 554, L111, doi: 10.1086/320935

Ferriz-Mas, A., Schmitt, D., & Schuessler, M. 1994, A&A, 289, 949

Frisch, U., Pouquet, A., Léorat, J., & A., M. 1975, J. Fluid Mech., 68, 769

Georgoulis, M. K., Rust, D. M., Pevtsov, A. A., Bernasconi, P. N., & Kuzanyan, K. M. 2009, ApJL, 705, L48, doi: 10.1088/0004-637X/705/1/L48

Getling, A. V., & Kosovichev, A. G. 2025, Astronomy Reports, 69, 144, doi: 10.1134/S1063772925701562

Getling, A. V., Kosovichev, A. G., & Zhao, J. 2021, ApJL, 908, L50, doi: 10.3847/2041-8213/abe45a

Gopalakrishnan, K., & Subramanian, K. 2023, ApJ, 943, 66, doi: 10.3847/1538-4357/aca808

Grigoryev, V., & Ermakova, L. 2025, Solar-Terrestrial Physics, 1, 5, doi: 10.12737/stp-111202501

Guerrero, G., Chatterjee, P., & Brandenburg, A. 2010, MNRAS, 409, 1619, doi: 10.1111/j.1365-2966.2010.17408.x

Hagino, M., & Sakurai, T. 2004, Publ. Astron. Soc. Japan, 56, 831

Hawkes, G., & Yeates, A. R. 2019, A&A, 631, A138, doi: 10.1051/0004-6361/201936475

Hoyng, P. 1993, A&A, 272, 321

Jakab, P., & Brandenburg, A. 2021, A&A, 647, A18, doi: 10.1051/0004-6361/202038564

Kitchatinov, L. L., & Pipin, V. V. 1993, A&A, 274, 647

Kleeorin, N., Moss, D., Rogachevskii, I., & Sokoloff, D. 2000, A&A, 361, L5

Kleeorin, N., & Rogachevskii, I. 1999, Phys. Rev.E, 59, 6724

Kleeorin, N., & Rogachevskii, I. 2022, MNRAS, 515, 5437, doi: 10.1093/mnras/stac2141

Kleeorin, N. I., & Ruzmaikin, A. A. 1982, Magnetohydrodynamics, 18, 116

Komm, R., Howe, R., & Hill, F. 2018, SoPh, 293, 145, doi: 10.1007/s11207-018-1365-7

Kosovichev, A. G., & Pipin, V. V. 2019, ApJ, 871, L20, doi: 10.3847/2041-8213/aafe82

Krause, F., & Rädler, K.-H. 1980, Mean-Field Magnetohydrodynamics and Dynamo Theory (Berlin: Akademie-Verlag), 271

Kutsenko, A. S., Abramenko, V. I., & Pevtsov, A. A. 2019, MNRAS, 484, 4393, doi: 10.1093/mnras/stz308

Kuzanyan, K., Yokoi, N., Georgoulis, M. K., & Stepanov, R., eds. 2024, Helicities in Geophysics, Astrophysics, and Beyond, Vol. 283, doi: 10.1002/9781119841715

Kuzanyan, K. M., Pipin, V. V., & Seehafer, N. 2006, Sol.Phys., 233, 185

Leka, K. D., Canfield, R. C., McClymont, A. N., & van Driel-Gesztelyi, L. 1996, ApJ, 462, 547, doi: 10.1086/177171

Liu, Y., Hoeksema, J. T., Bobra, M., et al. 2014, ApJ, 785, 13, doi: 10.1088/0004-637X/785/1/13

Mandal, K., Kosovichev, A. G., & Pipin, V. V. 2024, ApJ, 973, 36, doi: 10.3847/1538-4357/ad5f2c

Mitra, D., Candelaresi, S., Chatterjee, P., Tavakol, R., & Brandenburg, A. 2010, Astronomische Nachrichten, 331, 130, doi: 10.1002/asna.200911308

Mitra, D., Moss, D., Tavakol, R., & Brandenburg, A. 2011, A&A, 526, A138+, doi: 10.1051/0004-6361/201015637

Nagovitsyn, Y. A., Tlatov, A. G., & Nagovitsyna, E. Y. 2016, Astronomy Reports, 60, 831, doi: 10.1134/S1063772916090055

Norton, A., Howe, R., Upton, L., & Usoskin, I. 2023, SSRv, 219, 64, doi: 10.1007/s11214-023-01008-3

Pariat, E., Antiochos, S. K., & DeVore, C. R. 2009, ApJ, 691, 61, doi: 10.1088/0004-637X/691/1/61

Pariat, E., Démoulin, P., & Berger, M. A. 2005, A&A, 439, 1191, doi: 10.1051/0004-6361:20052663

Parker, E. 1955, Astrophys. J., 122, 293

Paxton, B., Bildsten, L., Dotter, A., et al. 2011, ApJS, 192, 3, doi: 10.1088/0067-0049/192/1/3

Perri, B., Brun, A. S., Strugarek, A., & Réville, V. 2021, ApJ, 910, 50, doi: 10.3847/1538-4357/abe2ac

Pevtsov, A. A., Bertello, L., Nagovitsyn, Y. A., Tlatov, A. G., & Pipin, V. V. 2021, Journal of Space Weather and Space Climate, 11, 4, doi: 10.1051/swsc/2020069

Pevtsov, A. A., Canfield, R. C., & Metcalf, T. R. 1994, ApJL, 425, L117, doi: 10.1086/187324

Pipin, V. 2024, SoPh, 299, 111, doi: 10.1007/s11207-024-02357-0

Pipin, V., & Kosovichev, A. 2024, ApJ, 962, 25, doi: 10.3847/1538-4357/ad1590

Pipin, V. V. 2008, Geophysical and Astrophysical Fluid Dynamics, 102, 21

—. 2022, MNRAS, 514, 1522, doi: 10.1093/mnras/stac1434

Pipin, V. V., & Kosovichev, A. G. 2019, ApJ, 887, 215, doi: 10.3847/1538-4357/ab5952

—. 2020, ApJ, 900, 26, doi: 10.3847/1538-4357/aba4ad

Pipin, V. V., Kosovichev, A. G., & Tomin, V. E. 2023, ApJ, 949, 7, doi: 10.3847/1538-4357/acaf69

Pipin, V. V., Sokoloff, D. D., Zhang, H., & Kuzanyan, K. M. 2013, ApJ, 768, 46, doi: 10.1088/0004-637X/768/1/46

Prior, C., & MacTaggart, D. 2019, Journal of Plasma Physics, 85, 775850201, doi: 10.1017/S0022377819000229

Prior, C., & Yeates, A. R. 2014, ApJ, 787, 100, doi: 10.1088/0004-637X/787/2/100

Seehafer, N. 1990, SoPh, 125, 219, doi: 10.1007/BF00158402

Sokoloff, D., Bao, S. D., Kleeorin, N., et al. 2006, Astron. Nachr., 327, 876

Sturrock, Z., Hood, A. W., Archontis, V., & McNeill, C. M. 2015, A&A, 582, A76, doi: 10.1051/0004-6361/201526521

Sun, Z., Li, T., Wang, Q., et al. 2024, A&A, 686, A148, doi: 10.1051/0004-6361/202348734

Tian, L., Liu, Y., Yang, J., & Alexander, D. 2005, SoPh, 229, 237, doi: 10.1007/s11207-005-6884-3

Toriumi, S., Hotta, H., & Kusano, K. 2024, ApJ, 975, 209, doi: 10.3847/1538-4357/ad7e1d

Toriumi, S., & Wang, H. 2019, Living Reviews in Solar Physics, 16, 3, doi: 10.1007/s41116-019-0019-7

Vidotto, A. A., Lehmann, L. T., Jardine, M., & Pevtsov, A. A. 2018, MNRAS, 480, 477, doi: 10.1093/mnras/sty1926

Warnecke, J., Brandenburg, A., & Mitra, D. 2011, A&A, 534, A11, doi: 10.1051/0004-6361/201117023

Yamamoto, T. T. 2011, PASJ, 63, 279, doi: 10.1093/pasj/63.1.279

Yeates, A., Cheung, M. M., Jiang, J., Petrovay, K., & Wang, Y.-M. 2023, SSRv, 219, 31, doi: 10.1007/s11214-023-00978-8

Zhang, H., Sakurai, T., Pevtsov, A., et al. 2010, MNRAS, 402, L30, doi: 10.1111/j.1745-3933.2009.00793.x

Zhang, H., Yang, S., Xu, H., et al. 2024, in Helicities in Geophysics, Astrophysics, and Beyond, ed. K. Kuzanyan, N. Yokoi, M. K. Georgoulis, & R. Stepanov, Vol. 283, 51–73, doi: 10.1002/9781119841715.ch4